Future snowfall in the Alps: Projections based on the EURO-CORDEX regional climate models

Prisco Frei [1], Sven Kotlarski [2,*], Mark A. Liniger [2], Christoph Schär [1]

[1] Institute for Atmospheric and Climate Sciences, ETH Zurich, CH-8006 Zurich, Switzerland
[2] Federal Office of Meteorology and Climatology, MeteoSwiss, CH-8058 Zurich-Airport, Switzerland

[*] Corresponding author: *sven.kotlarski@meteoswiss.ch*

Abstract. Twenty-first century snowfall changes over the European Alps are assessed based on high-resolution regional climate model (RCM) data made available through the EURO-CORDEX initiative. Fourteen different combinations of global and regional climate models with a target resolution of 12 km, and two different emission scenarios are considered. As raw snowfall amounts are not provided by all RCMs, a newly developed method to separate snowfall from total precipitation based on near-surface temperature conditions and accounting for subgrid-scale topographic variability is employed. The evaluation of the simulated snowfall amounts against an observation-based reference indicates the ability of RCMs to capture the main characteristics of the snowfall seasonal cycle and its elevation dependency, but also reveals considerable positive biases especially at high elevations. These biases can partly be removed by the application of a dedicated RCM bias adjustment that separately considers temperature and precipitation biases.

Snowfall projections reveal a robust signal of decreasing snowfall amounts over most parts of the Alps for both emission scenarios. Domain and multi-model mean decreases of mean September-May snowfall by the end of the century amount to -25% and -45% for RCP4.5 and RCP8.5, respectively. Snowfall in low-lying areas in the Alpine forelands could be reduced by more than -80%. These decreases are driven by the projected warming and are strongly connected to an important decrease of snowfall frequency and snowfall fraction and are also apparent for heavy snowfall events. In contrast, high-elevation regions could experience slight snowfall increases in mid-winter for both emission scenarios despite the general decrease of the snowfall fraction. These increases in mean and heavy snowfall can be explained by a general increase of winter precipitation and by the fact that, with increasing temperatures, climatologically cold areas are shifted into a temperature interval which favours higher snowfall intensities. In general, percentage changes of snowfall indices are robust with respect to the RCM postprocessing strategy employed: Similar results are obtained for raw, separated and separated + bias-adjusted snowfall amounts. Absolute changes, however, can differ among these three methods.

1 Introduction

Snow is an important resource for the Alpine regions, be it for tourism, hydropower generation, or water management (Abegg et al., 2007). According to the Swiss Federal Office of Energy (SFOE) hydropower generation accounts for approximately 55% of the Swiss electricity production (SFOE, 2014). Consideration of changes in snow climatology needs to address aspects of both snow cover and snowfall. In the recent past, an important decrease of the mean snow cover depth and duration in the Alps was observed (e.g, Laternser and Schneebeli, 2003; Marty, 2008; Scherrer et al., 2004). Projections of future snow cover changes based on climate model simulations indicate a further substantial reduction (Schmucki et al., 2015a; Steger et al., 2013), strongly linked to the expected rise of temperatures (e.g., CH2011, 2011; Gobiet et al., 2014). On regional and local scales rising temperatures exert a direct influence on snow cover in two ways: First, total snowfall sums are expected to decrease as a result of a lower probability for precipitation to fall as snow, implying a decreasing overall snowfall fraction (ratio between solid and total precipitation). Second, snow on the ground is subject to faster and accelerated melt. These warming-induced trends might be modulated, for instance, by changes in atmospheric circulation patterns.

Although the snowfall fraction is expected to decrease during the 21st century (e.g., Räisänen, 2016) extraordinary snowfall events can still leave a trail of destruction. A recent example was the winter 2013/2014 with record-breaking heavy snowfall events along the southern rim of the European Alps (e.g., Techel et al., 2015). The catastrophic effects of heavy snowfall range from avalanches and floods to road or rail damage. In extreme cases these events can even result in the weight-driven collapse of buildings or loss of human life (Marty and Blanchet, 2011). Also mean snowfall conditions, such as the mean number of snowfall days in a given period, can be of high relevance for road management (e.g. Zubler et al., 2015) or airport operation. Projections of future changes in snowfall, including mean and extreme conditions, are therefore highly relevant for long-term planning and adaptation purposes in order to assess and prevent related socio-economic impacts and costs.

21st century climate projections typically rely on comprehensive climate models. For large-scale projections, global climate models (GCMs) with a rather coarse spatial resolution of 100 km or more are used. To assess regional to local scale impacts, where typically a much higher spatial resolution is required, a GCM can be dynamically downscaled by nesting a regional climate model (RCM) over the specific domain of interest (Giorgi, 1990). In such a setup, the GCM provides the lateral and sea surface boundary conditions to the RCM. One advantage of climate models is their ability to estimate climate change in a physically based manner under different greenhouse gas (GHG) emission scenarios. With the Intergovernmental Panel on Climate Change's (IPCC) release of the Fifth Assessment Report (AR5; IPCC, 2013) the so-called representative concentration pathway (RCP) scenarios have been introduced (Moss et al., 2010). These specify GHG concentrations and corresponding emission pathways for several radiative forcing targets. To estimate inherent projection uncertainties, ensemble approaches employing different climate models, different greenhouse gas scenarios, and/or different initial conditions are being used (e.g., Deser et al., 2012; Hawkins and Sutton, 2009; Rummukainen, 2010).

Within the last few years several studies targeting the future global and European snowfall evolution based on climate model ensembles were carried out (e.g., de Vries et al., 2013; de Vries et al., 2014; Krasting et al., 2013; O'Gorman, 2014; Piazza et al., 2014; Räisänen, 2016; Soncini and Bocchiola, 2011). Most of these analyses are based on GCM output or older generations of RCM ensembles at comparatively low spatial resolution, which are not able to properly resolve snowfall events over regions with complex topography. New generations of high resolution RCMs are a first step toward an improvement on this issue. This is in particular true for the most recent high-resolution regional climate change scenarios produced by the global CORDEX initiative (Giorgi et al., 2009) and its European branch EURO-CORDEX (Jacob et al., 2014). The present work aims to exploit this recently established mutli-model archive with respect to future snowfall conditions over the area of the European Alps. It thereby complements the existing works of Piazza et al. (2014) and de Vries et al. (2014). These two works also exploit comparatively high-resolved RCM experiments but with a smaller focus domain in the case of Piazza et al. (2014; French Alps only) and based on a single-model ensemble with a comparatively small ensemble size (eight members) in the case of de Vries et al. (2014).

In general and on decadal to centennial time scales, two main drivers of future snowfall changes over the European Alps with competing effects on snowfall amounts are apparent from the available literature: (1) Mean winter precipitation is expected to increase over most parts of the European Alps and in most EURO-CORDEX experiments (e.g., Rajczak et al., 2017; Smiatek et al., 2016) which in principle could lead to higher snowfall amounts. (2) Temperatures are projected to considerably rise throughout the year (e.g., Gobiet et al., 2014; Smiatek et al., 2016; Steger et al., 2013) with the general effect of a decreasing snowfall frequency and fraction, thus potentially leading to a reduction in overall snowfall amounts. Separating the above two competing factors is one of the targets of the current study. A potential complication is that changes in daily precipitation frequency (events with precipitation > 1 mm/day) and precipitation intensity (average amount on wet days) can change in a counteracting manner (e.g., Fischer et al., 2015; Rajczak et al., 2013), and that relative changes are not uniform across the event category (e.g.; Fischer and Knutti, 2016; Rajczak et al., 2017).

We here try to shed more light on these issues by addressing the following main objectives:

Snowfall separation on the RCM grid. Raw snowfall outputs are not available for all members of the EURO-CORDEX RCM ensemble. Therefore, an adequate snowfall separation technique, i.e., the derivation of snowfall amounts based on readily available daily near-surface air temperature and precipitation data, is required. Furthermore, we seek for a snowfall separation method that accounts for the topographic subgrid-scale variability of snowfall on the RCM grid.

Snowfall bias adjustment. Even the latest generation of RCMs is known to suffer from systematic model biases (e.g., Kotlarski et al., 2014). In GCM-driven setups as employed within the present work these might partly be inherited from the driving GCM. To remove such systematic biases in temperature and precipitation, a dedicated bias adjustment method is developed and employed in the present work. To assess its performance and applicability, different snowfall indices in the bias-adjusted and not bias-adjusted output are compared against observation-based estimates.

116 **Snowfall projections for the late 21st century.** Climate change signals for various snowfall indices
117 over the Alpine domain and for specific elevation intervals, derived by a comparison of 30-year control
118 and scenario periods, are analysed under the assumption of the RCP8.5 emission scenario. In
119 addition, we aim to identify and quantify the main drivers of future snowfall changes and, in order to
120 assess emission scenario uncertainties, compare RCP8.5-based results with experiments assuming
121 the more moderate RCP4.5 emission scenario. Snowfall projections are generally based on three
122 different datasets: (1) raw RCM snowfall where available, (2) RCM snowfall separated from simulated
123 temperature and precipitation, and (3) RCM snowfall separated from simulated temperature and
124 precipitation and additionally bias-adjusted. While all three estimates are compared for the basic
125 snowfall indices in order to assess the robustness of the projections, more detailed analyses are
126 based on dataset (3) only.

127 In addition and as preparatory analysis, we carry out a basic evaluation of RCM-simulated snowfall
128 amounts. This evaluation, however, is subject to considerable uncertainties as a high-quality
129 observation-based reference at the required spatial scale is not available, and the focus of the present
130 work is laid on snowfall projections.

131 The article is structured as follows: Section 2 describes the data used and methods employed. In
132 Sections 3 and 4 results of the bias adjustment approach and snowfall projections for the late 21st
133 century are shown, respectively. The latter are further discussed in Section 5 while overall conclusions
134 and a brief outlook are provided in Section 6. Additional supporting figures are provided in the
135 Supplementary Material (prefix 'S' in figure numbers).

136 **2 Data and methods**

137 **2.1 Observational data**

138 To estimate the reference fine-scale snowfall, two gridded data sets, one for precipitation and one for
139 temperature, derived from station observations and covering the area of Switzerland are used. Both
140 data sets are available on a daily basis with a horizontal resolution of 2 km for the entire evaluation
141 period 1971-2005 (see Sec. 2.3).

142 The gridded precipitation data set (RhiresD) represents a daily analysis based on a high-resolution
143 rain-gauge network (MeteoSwiss, 2013a) consisting of more than 400 stations that have a balanced
144 distribution in the horizontal but under-represent high altitudes (Frei and Schär, 1998; Isotta et al.,
145 2014; Konzelmann et al., 2007). Albeit the data set's resolution of 2 km, the effective grid resolution as
146 represented by the mean inter-station distance is about 15 - 20 km and thus comparable to the
147 nominal resolution of the available climate model data (see Sec. 2.2). The dataset has not been
148 corrected for the systematic measurement bias of rain gauges (e.g., Neff, 1977; Sevruk, 1985; Yang et
149 al., 1999).

150 The gridded near-surface air temperature (from now on simply referred to as *temperature*) data set
151 (TabsD) utilises a set of approx. 90 homogeneous long-term station series (MeteoSwiss, 2013b).
152 Despite the high quality of the underlying station series, errors might be introduced by unresolved

153 scales, an uneven spatial distribution and interpolation uncertainty (Frei, 2014). The unresolved effects
154 of land cover or local topography, for instance, probably lead to an underestimation of spatial
155 variability. Also note that, while RhiresD provides daily precipitation sums aggregated from 6 UTC to 6
156 UTC of the following day, TabsD is a true daily temperature average from midnight UTC to midnight
157 UTC. Due to a high temporal autocorrelation of daily mean temperature this slight inconsistency in the
158 reference interval of the daily temperature and precipitation grids is expected to not systematically
159 influence our analysis.

160 In addition to the gridded temperature and precipitation datasets and in order to validate simulated raw
161 snowfall amounts station-based observations of fresh snow sums (snow depth) at daily resolution from
162 29 stations in Switzerland with data available for at least 80% of the evaluation period 1971-2005 are
163 employed.

164 **2.2 Climate model data**

165 In terms of climate model data we exploit a recent ensemble of regional climate projections made
166 available by EURO-CORDEX (www.euro-cordex.net), the European branch of the World Climate
167 Research Programme's CORDEX initiative (www.cordex.org; Giorgi et al., 2009). RCM simulations for
168 the European domain were run at a resolution of approximately 50 km (EUR-44) and 12 km (EUR-11)
169 with both re-analysis boundary forcing (Kotlarski et al., 2014; Vautard et al., 2013) and GCM forcing
170 (Jacob et al., 2014). We here disregard the reanalysis-driven experiments and employ the GCM-driven
171 simulations only. These include historical control simulations and future projections based on RCP
172 greenhouse gas and aerosol emission scenarios. We employ daily averaged model output of GCM-
173 driven EUR-11 simulations that were available in December 2016 and for which control, RCP4.5 and
174 RCP8.5 runs are provided. We hence exclusively focus on the higher resolved EUR-11 simulations
175 and disregard the coarser EUR-44 ensemble due to the apparent added value of the EUR-11
176 ensemble with respect to regional-scale climate features in the complex topographic setting of the
177 European Alps (e.g., Giorgi et al., 2016; Torma et al., 2015). Out of the entire set of available EURO-
178 CORDEX simulations, several GCM-RCM chains were either completely or partially removed from our
179 analysis, resulting in a full set of 14 GCM-RCM combinations and a reduced set of 12 combinations
180 only (Table 1). Reasons for removal are the existence of several realisations (MPI-ESM-REMO; only
181 one realisation has been used) and simulation deficiencies that potentially affect our analysis
182 (HadGEM2-RACMO, EC-EARTH-RACMO and IPSL-WRF). Further details on these issues are
183 provided in the Supplementary Material, Part B.

184 It is important to note that each of the RCMs considered uses an individual topography field. Model
185 topographies for a given grid cell might therefore considerably differ from each other, and also from the
186 observation-based orography. It is therefore not meaningful to compare snowfall values at individual
187 grid cells since the latter might be situated at different elevations. For this reason most analyses of the
188 present work were carried out as a function of elevation, i.e., by averaging quantities over distinct
189 elevation intervals.

2.3 Analysis domain and periods

The arc-shaped European Alps - with a West-East extent of roughly 1200 km , a total of area 190'000 km^2 and a peak elevation of 4810 m a.s.l. (Mont Blanc) - are the highest and most prominent mountain range which is entirely situated in Europe. In the present work, two different analysis domains are used. The evaluation of the bias adjustment approach depends on the observational data sets RhiresD and TabsD (see Sec. 2.1). As these cover Switzerland only, the evaluation part of the study (Sec. 3) is constrained to the Swiss domain (Fig. 1, bold line). For the analysis of projected changes of different snowfall indices (Sec. 4 and 5) a larger domain covering the entire Alpine crest with its forelands is considered (Fig. 1, coloured region).

Our analysis is based on three different time intervals. The evaluation period (EVAL) 1971-2005 is used for the calibration and validation of the bias adjustment approach. Future changes of snowfall indices are computed by comparing a present-day control period (1981-2010, CTRL) to a future scenario period at the end of the 21st century (2070-2099, SCEN). For all periods (EVAL, CTRL and SCEN), the summer months June, July and August (JJA) are excluded from the analysis. In addition to seasonal mean snowfall conditions, i.e., averages over the nine-month period from September to May, we also analyse the seasonal cycle of individual snowfall indices at monthly resolution.

2.4 Analysed snowfall indices and change signals

A set of six different snowfall indices is considered (Tab. 2). Mean snowfall (S_{mean}) refers to the (spatio-)temporally-averaged snowfall amount in mm SWE (note that from this point on we will use the term "mm" as a synonym for "mm SWE" as unit of several snowfall indices). The two indices heavy snowfall (S_{q99}) and maximum 1-day snowfall (S_{1d}) allow the assessment of projected changes in heavy snowfall events and amounts. S_{1d} is derived by averaging maximum 1-day snowfall amounts over all individual months/seasons of a given time period (i.e., by averaging 30 maximum values in the case of the CTRL and SCEN period), while S_{q99} is calculated from the grid point-based 99th all-day snowfall percentile of the daily probability density function (PDF) for the entire time period considered. We use all-day percentiles as the use of wet-day percentiles leads to conditional statements that are often misleading (see the analysis in Schär et al. 2016). Note that the underlying number of days differs for seasonal (September-May) and monthly analyses. Snowfall frequency (S_{freq}) and mean snowfall intensity (S_{int}) are based on a wet-day threshold of 1 mm/day and provide additional information about the distribution and magnitude of snowfall events, while the snowfall fraction (S_{frac}) describes the ratio of solid precipitation to total precipitation. As climate models tend to suffer from too high occurrence of drizzle and as small precipitation amounts are difficult to measure, daily precipitation values smaller or equal to 0.1 mm were set to zero in both the observations and the simulations prior to the remaining analyses.

Projections are assessed by calculating two different types of changes between the CTRL and the SCEN period. The absolute change signal (Δ) of a particular snowfall index X (see Tab.2)

$$\Delta X = X_{SCEN} - X_{CTRL} \tag{1}$$

227 and the relative change signal (δ) which describes the change of the snowfall index as a percentage of
228 its CTRL period value

$$\delta X = \left(\frac{X_{SCEN}}{X_{CTRL}} - 1\right) \cdot 100 \tag{2}$$

230 To prevent erroneous data interpretation due to possibly large relative changes of small CTRL values,
231 certain grid boxes were masked out before calculating and averaging the signal of change. This
232 filtering was done by setting threshold values for individual indices and statistics (Tab. 2).

2.5 Separating snowfall from total precipitation

234 Due to (a) the lack of a gridded observational snowfall data set and (b) the fact that not all EURO-
235 CORDEX RCMs provide raw snowfall as an output variable, a method to separate solid from total
236 precipitation depending on near-surface temperature conditions is developed. The simplest approach
237 to separate snowfall from total precipitation is to fractionate the two phases binary by applying a
238 constant snow fractionation temperature (e.g., de Vries et al., 2014; Schmucki et al., 2015a; Zubler et
239 al., 2014). More sophisticated methods estimate the snow fraction f_s dependence on air temperature
240 with linear or logistic relations (e.g., Kienzle, 2008; McAfee et al., 2014). In our case, the different
241 horizontal resolutions of the observational (high resolution of 2 km) and simulated (coarser resolution
242 of 12 km) data sets further complicate a proper comparison of the respective snowfall amounts. Thus,
243 we explicitly analysed the snowfall amount dependency on the grid resolution and exploited
244 possibilities for including subgrid-scale variability in snowfall separation. This approach is important as
245 especially in Alpine terrain a strong subgrid-scale variability of near-surface temperatures due to
246 orographic variability has to be expected, with corresponding effects on the subgrid-scale snowfall
247 fraction.

248 For this preparatory analysis, which is entirely based on observational data, a reference snowfall is
249 derived. It is based on the approximation of snowfall by application of a fixed temperature threshold to
250 daily total precipitation amounts on the high resolution observational grid (2 km) and will be termed
251 *Subgrid method* thereafter: First, the daily snowfall S' at each grid point of the observational data set at
252 high resolution (2 km) is derived by applying a snow fractionation temperature T^*=2°C. The whole
253 daily precipitation amount P' is accounted for as snow S' (i.e., f_s=100%) for days with daily mean
254 temperature $T' \leq T^*$. For days with $T' > T^*$, S' is set to zero and P' is attributed as rain (i.e., f_s=0%). This
255 threshold approach with a fractionation temperature of 2°C corresponds to the one applied in previous
256 works and results appear to be in good agreement with station-based snowfall measurements (e.g.,
257 Zubler et al., 2014). The coarse grid (12 km) reference snowfall S_{SG} is determined by averaging the
258 sum of separated daily high resolution S' over all n high-resolution grid points i located within a specific
259 coarse grid point k. I.e., at each coarse grid point k

$$S_{SG} = \frac{1}{n} \cdot \sum_{i=1}^{n} P'_i \left[T'_i \leq T^* \right] = \frac{1}{n} \sum_{i=1}^{n} S'_i \tag{3}$$

261 For comparison, the same binary fractionation method with a temperature threshold of T^*=2°C is
262 directly applied on the coarse 12 km grid (*Binary method*). For this purpose, total precipitation P' and
263 daily mean temperature T' of the high-resolution data are conservatively remapped to the coarse grid

leading to P and T, respectively. Compared to the *Subgrid method*, the *Binary method* neglects any subgrid-scale variability of the snowfall fraction. As a result, the *Binary method* underestimates S_{mean} and overestimates S_{q99} for most elevation intervals (Fig. 2). The underestimation of S_{mean} can be explained by the fact that even for a coarse grid temperature above T^* individual high-elevation subgrid cells (at which $T' \leq T^*$) can receive substantial snowfall amounts. As positive precipitation-elevation gradients can be assumed for most parts of the domain (larger total precipitation at high elevations; see e.g. Kotlarski et al., 2012 and Kotlarski et al., 2015 for an Alpine-scale assessment) the neglect of subgrid-scale snowfall variation in the *Binary method* hence leads to a systematic underestimation of mean snowfall compared to the *Subgrid method*. Furthermore, following O'Gorman (2014), heavy snowfall events are expected to occur in a narrow temperature range below the rain-snow transition. As the *Binary method* in these temperature ranges always leads to a snowfall fraction of 100%, too large S_{q99} values would result.

To take into account these subgrid-scale effects, a more sophisticated approach – referred to as the *Richards method* – is developed here. This method is based upon a generalised logistic regression (Richards, 1959). Here, we apply this regression to relate the surface temperature T to the snow fraction f_s by accounting for the topographic subgrid-scale variability. At each coarse grid-point k, the *Richards method*-based snowfall fraction $f_{s,RI}$ for a given day is hence computed as follows:

$$f_{s,RI}(T_k) = \frac{1}{\left[1+C_k \cdot e^{D_k \cdot (T_k - T^*)}\right]^{\frac{1}{C_k}}} \tag{4}$$

with C as the point of inflexion (denoting the point with largest slope), and D the growth rate (reflecting the mean slope). T_k is the daily mean temperature of the corresponding coarse grid box k and $T^*=2°C$ the snow fractionation temperature. First, we estimate the two parameters C and D of Equation 4 for each single coarse grid point k by minimizing the least-square distance to the f_s values derived by the *Subgrid method* via the reference snowfall S_{SG} (local fit). Second, C and D are expressed as a function of the topographic standard deviation σ_h of the corresponding coarse resolution grid point only (Fig. S1; global fit). This makes it possible to define empirical functions for both C and D that can be used for all grid points k in the Alpine domain and that depend on σ_h only.

$$\sigma_{h,k} = \sqrt{\frac{\sum_i^n (h_i - \overline{h_k})^2}{n-1}} \tag{5}$$

$$C_k = \frac{1}{(E - \sigma_{h,k} \cdot F)} \tag{6}$$

$$D_k = G \cdot \sigma_{h,k}^{-H} \tag{7}$$

Through a minimisation of the least square differences the constant parameters in Equations 6 and 7 are calibrated over the domain of Switzerland and using daily data from the period September to May 1971-2005 leading to values of E=1.148336, F=0.000966 m^{-1}, G=143.84113 °C^{-1} and H=0.8769335. Note that σ_h is sensitive to the resolution of the two grids to be compared (cf. Eq. 5). It is a measure for the uniformity of the underlying topography and has been computed based on the high-resolution GTOPO30 digital elevation model (https://lta.cr.usgs.gov/GTOPO30) aggregated to a regular grid of

299   1.25 arc seconds (about 2 km) which reflects the spatial resolution of the observed temperature and

300   precipitation grids (cf. Sec. 2.1). Small values of σ_h indicate a low subgrid-scale topographic variability,

301   such as in the Swiss low-lands, while high values result from non-uniform elevation distributions, such

302   as in areas of inner Alpine valleys. σ_h as derived from GTOPO30 might be different from the subgrid-

303   scale topographic variance employed by the climate models themselves, which is however not

304   relevant here as only grid cell-averaged model output is analysed while σ_h is regarded as a proper

305   estimate of subgrid-scale variability.

306   Figure S1 (panel c) provides an example of the relation between daily mean temperature and daily

307   snow fraction f_s for grid cells with topographical standard deviations of 50 m and 500 m, respectively.

308   The snowfall amount S_{RI} for a particular day and a particular coarse grid box is finally obtained by

309   multiplying the corresponding $f_{s,RI}$ and P values. A comparison with the *Subgrid method* yields very

310   similar results. For both indices S_{mean} and $S_{q99,}$ mean ratios across all elevation intervals are close to 1

311   (Fig. 2). At single grid points, maximum deviations are not larger than 1±0.1. Note that for this

312   comparison calibration and validation period are identical (EVAL period). Based on this analysis, it has

313   been decided to separate snowfall according to the *Richards method* throughout this work in both the

314   observations and in the RCMs. The observation-based snowfall estimate obtained by applying the

315   *Richards method* to the observational temperature and precipitation grids after spatial aggregation to

316   the 0.11° RCM resolution will serve as reference for the RCM bias adjustment and will be termed

317   *reference* hereafter. One needs to bear in mind that the parameters C and D of the Richards method

318   were fitted for the Swiss domain only and were later on applied to the entire Alpine domain (cf. Fig. 1).

2.6 Bias adjustment approach

320   Previous work has revealed partly substantial temperature and precipitation biases of the EURO-

321   CORDEX RCMs over the Alps (e.g. Kotlarski et al., 2014; Smiatek et al., 2016), and one has to expect

322   that the separated snowfall amounts are biased too. This would especially hamper the interpretation of

323   absolute climate change signals of the considered snow indices. We therefore explore possibilities to

324   bias-adjust the simulated snowfall amounts and to directly integrate this bias adjustment into the

325   snowfall separation framework of Section 2.5. Note that we deliberately employ the term *bias*

326   *adjustment* as opposed to *bias correction* to make clear that only certain aspects of the snowfall

327   climate are adjusted and that the resulting dataset might be subject to remaining inaccuracies.

328   A simple two-step approach that separately accounts for precipitation and temperature biases and

329   their respective influence on snowfall is chosen. The separate consideration of temperature and

330   precipitation biases allows for a more physically-based bias adjustment of snowfall amounts: Due to

331   the temperature dependency of snowfall occurrence, snowfall biases of a given climate model cannot

332   be expected to remain constant under changing climate conditions. For instance, a climate model with

333   a given temperature bias might pass the snow-rain temperature threshold earlier or later than reality

334   during the general warming process. Hence, traditional bias adjustment approaches based only on a

335   comparison of observed and simulated snowfall amounts in the historical climate would possibly fail

336   due to a non-stationary bias structure. The bias adjustment is calibrated in the EVAL period for each

337   individual GCM-RCM chain and over the region of Switzerland, and is then applied to both the CTRL

and SCEN period of each chain and for the entire Alpine domain. To be consistent in terms of horizontal grid spacing, the observational data sets RhiresD and TabsD (see Sec. 2.1) are conservatively regridded to the RCM resolution beforehand.

In a first step, total simulated precipitation is adjusted by introducing an elevation-dependent adjustment factor which adjusts precipitation biases regardless of temperature. For this purpose, mean precipitation ratios (RCM simulation divided by observational analysis) for 250 m elevation intervals are calculated (Fig. S3). An almost linear relationship of these ratios with elevation is found. Thus, a linear regression between the intervals from 250 m a.s.l. to 2750 m a.s.l. is used for each model chain separately to estimate a robust adjustment factor. As the number of both RCM grid points and measurement stations at very high elevations (>2750 m a.s.l.) is small (Sec. 2.1; Fig. S2) and biases are subject to a considerable sampling uncertainty, these elevations are not considered in the regression. Overall the fits are surprisingly precise except for the altitude bins above 2000 m (Fig. S3). The precipitation adjustment factors (P_{AF}) for a given elevation are then obtained as the inverse of the fitted precipitation ratios. Multiplying simulated precipitation P with P_{AF} for the respective model chain and elevation results in the adjusted precipitation:

$$P_{adj} = P \cdot P_{AF} \tag{8}$$

For a given GCM-RCM chain and for each elevation interval, the spatially and temporally averaged corrected total precipitation P_{adj} approximately corresponds to the observation-based estimate in the EVAL period.

In the second step of the bias adjustment procedure, temperature biases are accounted for. For this purpose the initial snow fractionation temperature T*=2°C of the Richards separation method (see Sec 2.5) is shifted to the value T_a^* for which the spatially (Swiss domain) and temporally (September to May) averaged simulated snowfall amounts for elevations below 2750 m a.s.l. match the respective observation-based reference (see above). Compared to the adjustment of total precipitation, T_a^* is chosen independent of elevation but separately for each GCM-RCM chain, in order to avoid over-parameterization and to not over-interpret the elevation dependency of mean snowfall in the snowfall reference grid. After this second step of the bias adjustment, the spatially and temporally averaged simulated snowfall amounts below 2750 m a.s.l. match the reference by definition. Hence, the employed simple bias adjustment procedure adjusts domain-mean snowfall biases averaged over the entire season from September to May. It does, however, not correct for biases in the spatial snowfall pattern, in the seasonal cycle, or in the temporal distribution of daily values. Note that, as the underlying high-resolution data sets are available over Switzerland only, the calibration of the bias adjustment methodology is correspondingly restricted, but the adjustment is then applied to the whole Alpine domain. This approach is justified as elevation-dependent mean winter precipitation and temperature biases of the RCMs employed - assessed by comparison against the coarser-resolved EOBS reference dataset (Haylock et al., 2008) - are very similar for Switzerland and for the entire Alpine analysis domain (Figs. S4 and S5).

3 Evaluation

3.1 RCM raw snowfall

We first carry out an illustrative comparison of RCM raw snowfall amounts (for those simulations only that directly provide snowfall flux) against station observations of snowfall in order to determine whether the simulated RCM snowfall climate contains valid information despite systematic biases. To this end, simulated raw snowfall amounts of seven EURO-CORDEX simulations of the reduced set (Tab. 1) averaged over 250 m-elevation intervals and over the range 950 – 1650 m a.s.l. are compared against observations of measured fresh snow sums from 29 MeteoSwiss stations (Sec. 2.1).. For this purpose a mean snow density of 100 kg/m^3 for the conversion from measured snow depth to water equivalent is assumed. Note that this simple validation is subject to considerable uncertainties as it does not explicitly correct for the scale and elevation gap between grid-cell based RCM output and single-site observations. Especially in complex terrain and for exposed sites, point measurements of snow depth might be non-representative for larger-scale conditions (e.g., Grünewald and Lehning, 2015). Also, the conversion from snow depth to snow water equivalent is of approximate nature only, and fresh snow sums might furthermore misrepresent true snowfall in case that snow melt or snow drift occurs between two snow depth readings.

At low elevations simulated mean September-May raw snowfall sums match the observations well while differences are larger aloft (Fig. 3a). The positive bias at high elevations might arise from the fact that (the very few) observations were made at specific locations while simulated grid point values of the corresponding elevation interval might be located in different areas of Switzerland. It might also be explained by positive RCM precipitation and negative RCM temperature biases at high elevations of the Alps (e.g., Kotlarski et al., 2015). Also note that, in general, the total high-elevation area of the Alpine analysis domain is small and elevations above 2500 m represent less than 5% of the total area (Fig. S2). Both model-based and observation-based estimates for high-elevations are hence subject to a considerable sampling uncertainty and are likely to be less robust than estimates for lower elevations.

At lower elevations, the station network is geographically more balanced and the observations are probably more representative of the respective elevation interval. Despite a clear positive snowfall bias in mid-winter, the RCMs are generally able to reproduce the mean seasonal cycle of snowfall for elevations between 950 m a.s.l. - 1650 m a.s.l. (Fig. 3b). The fact that the major patterns of both the snowfall-elevation relationship and the mean seasonal snowfall cycle are well represented indicates the general and physically consistent applicability of RCM output to assess future changes in mean and heavy Alpine snowfall. However, substantial biases in snowfall amounts are apparent and a bias adjustment of simulated snowfall seems to be required prior to the analysis of climate change signals of individual snowfall indices.

3.2 Evaluation of the reference snowfall

The snowfall separation employing the *Richards method* (Sec. 2.5) and, as a consequence, also the bias adjustment (Sec. 2.6) make use of the 2 km reference snowfall grid derived by employing the

413   *Subgrid method* on the observed temperature and precipitation grids. Hence, the final results of this
414   study could to some extent be influenced by inaccuracies and uncertainties of the reference snowfall
415   grid itself. In order to assess the quality of the latter and in absence of a further observation-based
416   reference we here present an approximate evaluation.

417   First, the reference snowfall grid is evaluated against fresh snow sums at the 29 Swiss stations that
418   are also used for evaluating RCM raw snowfall. Note the limitations of such a comparison as outlined
419   in Chapter 3.1. The comparison of black and red markers and lines in Figure 3 indicates a good
420   agreement of mean snowfall at individual elevation intervals (left panel) as well for the mean annual
421   cycle of snowfall at medium elevations (right panel). The reference snowfall grid is obviously a good
422   approximation of site-scale fresh snow sums. Note that similarly to the RCM raw snowfall evaluation,
423   all 2 km reference snowfall grid cells in the respective elevation interval are considered. The good
424   agreement, however, still holds if only those 2 km grid cells covering the 29 site locations are
425   considered (not shown here).

426   Second, both the 2 km reference snowfall grid and the 0.11° reference snowfall grid obtained by
427   employing the Richards method to aggregated temperature and precipitation values (Sec. 2.5) are
428   compared against the gridded HISTALP dataset of solid precipitation (Chimani et al., 2011). The latter
429   is provided at a monthly resolution on a 5' grid covering the Greater Alpine Region. It is based on
430   monthly snowfall fraction estimates that are used to scale a gridded dataset of total precipitation. The
431   comparison of the three datasets for the region of Switzerland (for which the 2 km reference snowfall
432   is available) in the EVAL period 1971-2005 yields an approximate agreement of both the magnitude of
433   mean winter snowfall and its spatial pattern (Fig. S6). The three data sets differ with respect to their
434   spatial resolution but all show a clear dependency of snowfall on topography and mean September-
435   May snowfall sums above 1000 mm over most parts of the Alpine ridge. Climatologically warm and dry
436   valleys, on the other hand, are represented by minor snowfall amounts of less than 400 mm only.

437   As mentioned before these evaluations of the reference snowfall grid are subject to uncertainties and,
438   furthermore, they only cover mean snowfall amounts. However, they provide basic confidence in the
439   applicability of the reference snowfall grid for the purposes of snowfall separation and bias adjustment
440   in the frame of the present study.

441

442   **3.3 Calibration of bias adjustment**

443   The analysis of total precipitation ratios (RCM simulations with respect to observations) for the EVAL
444   period, which are computed to carry out the first step of the bias adjustment procedure, reveals
445   substantial elevation dependencies. All simulations tend to overestimate total precipitation at high
446   elevations (Fig. S3). This fact might ultimately be connected to an overestimation of surface snow
447   amount in several EURO-CORDEX RCMs as reported by Terzago et al. (2017). As the precipitation
448   ratio between simulations and observations depends approximately linearly on elevation, the
449   calculation of P_{AF} via a linear regression of the ratios against elevation (see Sec. 2.6) seems
450   reasonable. By taking the inverse of this linear relation, P_{AF} for every model and elevation can be

451 derived. For the CCLM simulations, these correction factors do not vary much with height, while P_{AF}
452 for MPI-ESM - REMO and EC-EARTH - HIRHAM is much larger than 1 in low lying areas, indicating a
453 substantial underestimation of observed precipitation sums (Fig. 4a). However, for most elevations
454 and simulations, P_{AF} is generally smaller than 1, i.e., total precipitation is overestimated by the models.
455 Similar model biases in the winter and spring seasons have already been reported in previous works
456 (e.g., Rajczak et al., 2017; Smiatek et al., 2016). Especially at high elevations, these apparent positive
457 precipitation biases could be related to observational undercatch, i.e., an underestimation of true
458 precipitation sums by the observational analysis. Frei et al. (2003) estimated seasonal Alpine
459 precipitation undercatch for three elevation intervals. Results show that measurement biases are
460 largest in winter and increase with altitude. However, a potential undercatch (with a maximum of
461 around 40% at high elevations in winter; Frei et al., 2003) can only partly explain the often substantial
462 overestimation of precipitation found in the present work.

463 After applying P_{AF} to the daily precipitation fields, a snowfall fractionation at the initial T^* of 2 °C (see
464 Eq. (4)) would lead to a snowfall excess in all 12 simulations as models typically experience a cold
465 winter temperature bias. To match the observation-based and spatio-temporally averaged reference
466 snowfall below 2750 m a.s.l., T^* for all models needs to be decreased during the second step of the
467 bias adjustment (Fig. 4b). The adjusted T^*_a values indicate a clear positive relation with the mean
468 temperature bias in the EVAL period. This feature is expected since the stronger a particular model's
469 cold bias the stronger the required adjustment of the snow fractionation temperature T^* towards lower
470 values in order to avoid a positive snowfall bias. Various reasons for the scatter around a simple linear
471 relation in Figure 4b can be thought of. These include remaining spatial inaccuracies of the corrected
472 precipitation grid, elevation-dependent temperature biases and misrepresented temperature-
473 precipitation relationships at daily scale. Note that precipitation and temperature biases heavily
474 depend on the GCM-RCM chain and seem to be rather independent from each other. Concerning the
475 partly substantial temperature biases of the EURO-CORDEX models shown in Figure 4b, their
476 magnitude largely agrees with Kotlarski et al. (2014; in reanalysis-driven simulations) and Smiatek et
477 al. (2016).

478 **3.4 Evaluation of snowfall indices**

479 We next assess the performance of the bias adjustment procedure by comparing snowfall indices
480 derived from separated and bias-adjusted RCM snowfall amounts against the observation-based
481 reference. The period for which this comparison is carried out is EVAL, i.e., it is identical to the
482 calibration period of the bias adjustment. We hence do not intend a classical cross validation exercise
483 with separate calibration and validation periods, but try to answer the following two questions: (a)
484 Which aspects of the Alpine snowfall climate are adjusted, and (b) for which aspects do biases remain
485 even after application of the bias adjustment procedure.

486 Figure 5 shows the evaluation results of the six snowfall indices based on the separated and not bias-
487 adjusted simulated snowfall (RCM$_{sep+nba}$), and the separated and bias-adjusted simulated snowfall
488 (RCM$_{sep+ba}$). In the first case the snowfall separation of raw precipitation is performed with $T^*=2°C$,
489 while in the second case precipitation is adjusted and the separation is performed with a bias-adjusted

490   temperature T^*_a. The first column represents the mean September to May statistics, while columns 2-4

491   depict the seasonal cycle at monthly resolution for three distinct elevation intervals.

492   The analysis of S_{mean} confirms that RCM_{sep+ba} is able to reproduce the observation-based reference in

493   the domain mean as well as in most individual elevation intervals. The domain-mean agreement is a

494   direct consequence of the design of the bias adjustment procedure (see above). $RCM_{sep+nba}$, on the

495   other hand, consistently overestimates S_{mean} by up to a factor of 2.5 as a consequence of positive

496   precipitation and negative temperature biases (cf. Fig. 4). Also the seasonal cycle of S_{mean} for

497   RCM_{sep+ba} yields a satisfying performance across all three elevation intervals, while $RCM_{sep+nba}$ tends

498   to produce too much snowfall over all months and reveals an increasing model spread with elevation.

499   For the full domain and elevations around 1000 m, the observation-based reference indicates a mean

500   S_{freq} of 20% between September and May. Up to 1000 m a.s.l. RCM_{sep+ba} reflects the increase of this

501   index with elevation adequately. However, towards higher elevations the approximately constant S_{freq}

502   of 30% in the reference is not captured by the simulation-derived snowfall. Notably during wintertime,

503   both RCM_{sep+ba} and $RCM_{sep+nba}$ produce too many snowfall days, i.e., overestimate snowfall frequency.

504   This feature is related to the fact that climate models typically tend to overestimate the wet day

505   frequency over the Alps especially in wintertime (Rajczak et al., 2013) and that the bias adjustment

506   procedure employed does not explicitly correct for potential biases in precipitation frequency. Due to

507   the link between mean snowfall on one side and snowfall frequency and mean intensity on the other

508   side, opposite results are obtained for the mean snowfall intensity S_{int}. RCM_{sep+ba} largely

509   underestimates mean intensities during snowfall days while $RCM_{sep+nba}$ typically better reflects the

510   reference. Nevertheless, deviations during winter months at mid-elevations are not negligible. Mean

511   September-May S_{frac} in the reference exponentially increases with elevation. This behaviour is

512   reproduced by both RCM_{sep+ba} and $RCM_{sep+nba}$. Notwithstanding, RCM_{sep+ba} results are more accurate

513   compared to $RCM_{sep+nba}$, which turns out to be biased towards too large snowfall fractions.

514   For the two heavy snowfall indices S_{q99} and S_{1d}, $RCM_{sep+nba}$ appears to typically match the reference

515   better than RCM_{sep+ba}. Especially at high elevations, RCM_{sep+ba} produces too low snowfall amounts.

516   This again illustrates the fact that the bias adjustment procedure is designed to adjust biases in mean

517   snowfall, but does not necessarily improve further aspects of the simulated snowfall climate.

518   The spatial patterns of S_{mean} for the 12 RCM_{sep+ba} simulations from September to May are presented in

519   Figure 6. The observational-based reference (lower-right panel) reveals a snowfall distribution with

520   highest values along the Alpine main ridge, whereas the Swiss plateau, Southern Ticino and main

521   valleys such as the Rhône and Rhine valley experience less snowfall. Almost all bias-adjusted models

522   are able to represent the overall picture with snow-poor lowlands and snow-rich Alpine regions.

523   Nevertheless substantial differences to the observations concerning the spatial snowfall pattern can

524   arise. EC-EARTH - HIRHAM, for example, is subject to a noisy structure. This could be the result of

525   frequent grid-cell storms connected to parameterisations struggling with complex topographies. Such

526   inaccuracies in the spatial pattern are not corrected for by our simple bias adjustment approach which

527   only targets domain-mean snowfall amounts at elevations below 2750 m a.s.l. and that does not

528   considerably modify the simulated spatial snowfall patterns.. Note that these patterns are obviously

529   strongly determined by the RCM itself and only slightly depend on the driving GCM (see, for instance,
530   the good agreement among the CCLM and the RCA simulations).

531   In summary, after applying the bias adjustment to the simulations most snowfall indices are fairly well
532   represented at elevations below 1000 m a.s.l.. With increasing altitude and smaller sample sizes in
533   terms of number of grid cells, reference and RCM_{sep+ba} diverge. This might be caused by the remaining
534   simulated overestimation of S_{freq} and an underestimation of S_{int}. While the bias adjustment approach
535   leads to a reduction of S_{int} due to the total precipitation adjustment, S_{freq} is only slightly modified by this
536   correction and by the adjustment of T^*. Nevertheless, these two parameters strongly influence other
537   snowfall indices. The counteracting effects of overestimated S_{freq} and underestimated S_{int} result in
538   appropriate amounts of S_{mean} whereas discrepancies for S_{q99} and S_{1d} are mainly driven by the
539   underestimation of S_{int}.

540   **4 Snowfall projections for the late 21st century**

541   For the study of climate change signals, the analysis domain is extended to the entire Alps (see Sec.
542   2.3). Due to the identified difficulties of bias-adjusting certain snowfall indices (see Sec 3.4), emphasis
543   is laid on relative signals of change (see Eq. 2). This type of change can be expected to be less
544   dependent on the remaining inaccuracies after the adjustment. If not stated otherwise, all results in
545   this Section are based on the RCM_{sep+ba} data, i.e., on separated and bias-adjusted RCM snowfall, and
546   on the RCP8.5 emission scenario. Depending on the type of analysis, either the full or the reduced
547   model set is used (see Tab. 1 and Supplementary Material, Part B).

548   Projections for seasonal S_{mean} show a considerable decrease over the entire Alpine domain (Fig. 7).
549   Most RCMs project largest percentage losses of more than 80% across the Alpine forelands and
550   especially in its topographic depressions such as the Po and Rhone valleys. Over the Alpine ridge,
551   reductions are smaller but still mostly negative. Elevated regions between Southeastern Switzerland,
552   Northern Italy and Austria seem to be least affected by the overall snowfall reduction. Some of the
553   simulations (e.g., CNRM-RCA, MPI-ESM-RCA or MPI-ESM-REMO) project only minor changes in
554   these regions. Experiments employing the same RCM but different driving GCMs (e.g. the four
555   simulations of RCA), but also experiments employing the same GCM but different RCMs (e.g. the four
556   simulations driven by EC-EARTH, though different realizations) can significantly disagree in regional-
557   scale change patterns and especially in the general magnitude of change. This highlights a strong
558   influence of both the driving GCMs and the RCMs themselves on snowfall changes, representing
559   effects of large-scale circulation and meso-scale response, respectively.

560   A more detailed analysis is provided in Fig. 8 which addresses the vertical and seasonal distribution of
561   snowfall changes. It reveals that relative (seasonal mean) changes of S_{mean} appear to be strongly
562   dependent on elevation (Fig.8, top left panel). The multi-model mean change ranges from -80% at low
563   elevations to -10% above 3000 m a.s.l.. Largest differences between neighbouring elevation intervals
564   are obtained from 750 m a.s.l. to 1500 m a.s.l.. Over the entire Alps, the results show a reduction of
565   S_{mean} by -35% to -55% with a multi-model mean of -45%. The multi-model spread appears to be rather
566   independent of elevation and is comparably small, confirming that, overall, the spatial distribution of

567 the change pattern is similar across all model chains (cf. Fig. 7). All simulations point to decreases
568 over the entire nine-month period September to May for the two elevation intervals <1000 m a.s.l. and
569 1000 to 2000 m a.s.l.. Above 2000 m a.s.l., individual simulations show an increase of S_{mean} by up to
570 20% in mid-winter which leads to a slightly positive change in the multi-model mean in January and
571 February.

572 Decreases of S_{freq} are very similar to changes in mean snowfall. Mean September-May changes are
573 largest below 1000 m a.s.l., while differences among elevation intervals become smaller at higher
574 elevations. In-between is a transition zone with rather strong changes with elevation, which
575 approximately corresponds to the mean elevation of the September-May zero-degree line in today's
576 climate (e.g., Ceppi et al., 2012; MeteoSchweiz, 2016). Individual simulations with large reductions in
577 S_{mean}, such as the RCA experiments, also project strongest declines in S_{freq}. In contrast, the mean
578 snowfall intensity S_{int} is subject to smallest percentage variations in our set of snowfall indices. Strong
579 percentage changes for some models in September are due to the small sample size (only few grid
580 points considered) and the low snowfall amounts in this month. Apart from mid elevations with
581 decreases of roughly -10%, mean intensities from September to May are projected to remain almost
582 unchanged by the end of the century. For both seasonal and monthly changes, model agreement is
583 best for high elevations while the multi-model spread is largest for the lowlands. Large model spread
584 at low elevations might be caused by the small number of grid points used for averaging over the
585 respective elevation interval, especially in autumn and spring.

586 Similar results are obtained for the heavy snowfall indices S_{q99} and S_{1d}. While percentage decreases
587 at lowermost elevations are even larger than for S_{mean}, losses at high elevations are less pronounced,
588 resulting in similar domain-mean change signals for heavy and mean snowfall. Substantial differences
589 between monthly δS_{q99} and δS_{1d} appear at elevations below 1000 m a.s.l.. Here, percentage losses of
590 S_{q99} are typically slightly more pronounced. Above 2000 m a.s.l. both indices appear to remain almost
591 constant between January and March with change signals close to zero. The multi-model mean
592 changes even hint to slight increases of both indices. Concerning changes in the snowfall fraction, i.e.,
593 in the relative contribution of snowfall to total precipitation, our results indicate that current seasonal
594 and domain mean S_{frac} might drop by about -50% (Fig. 8, lowermost row). Below 1000 m a.s.l., the
595 strength of the signal is almost independent of the month, and multi-model average changes of the
596 snow fraction of about -80% are obtained. At higher elevations changes during mid-winter are less
597 pronounced compared to autumn and spring but still negative.

598 **5 Discussion**

599 **5.1 Effect of temperature, snowfall frequency and intensity on snowfall changes**

600 The results in Section 4 indicate substantial changes of snowfall indices over the Alps in regional
601 climate projections. With complementary analyses presented in Figures 9 and 10 we shed more light
602 on the responsible mechanisms, especially concerning projected changes in mean and heavy
603 snowfall. For this purpose Figures 9a-b,e-f show the relationship of both mean and heavy snowfall
604 amounts in the CTRL period and their respective percentage changes with the climatological CTRL

temperature of the respective (climatological) month, elevation interval and GCM-RCM chain. For absolute amounts (S_{mean}, S_{q99}; Fig. 9a,e) a clear negative relation is found, i.e., the higher the CTRL temperature the lower the snowfall amounts. For S_{mean} the relation levels off at mean temperatures higher than about 6°C with mean snowfall amounts close to zero. For temperatures below about -6°C a considerable spread in snowfall amounts is obtained, i.e., mean temperature does not seem to be the controlling factor here. Relative changes of both quantities (Fig. 9b,f), however, are strongly controlled by the CTRL period's temperature level with losses close to 100% for warm climatic settings and partly increasing snowfall amounts for colder climates. This dependency of relative snowfall changes on CTRL temperature is in line with previous works addressing future snowfall changes on both hemispheric and regional scales (de Vries et al., 2014; Krasting et al., 2013; Räisänen, 2016). The spread of changes within a given CTRL temperature bin can presumably be explained by the respective warming magnitudes that differ between elevations, months and GCM-RCM chains. About half of this spread can be attributed to the month and the elevation alone (compare the spread of the black markers to the one of the red markers which indicate multi-model averages).

For most months and elevation intervals, percentage reductions in S_{mean} and S_{q99} reveal an almost linear relationship with δS_{freq} (Fig. 9c, g). The decrease of S_{freq} with future warming can be explained by a shift of the temperature probability distribution towards higher temperatures, leading to fewer days below the freezing level (Fig. 10, top row). Across the three elevation intervals <1000 m a.s.l., 1000-2000 m a.s.l. and > 2000 m a.s.l., relative changes in the number of days with temperatures below the freezing level (T≤0°C) are in the order of -65%, -40% and -20%, respectively (not shown). This approximately corresponds to the simulated decrease of S_{freq} (cf. Fig 8), which in turn, is of a similar magnitude as found in previous works addressing future snowfall changes in the Alps (Schmucki et al., 2015b; Zubler et al., 2014). Due to the general shift of the temperature distribution and the "loss" of very cold days (Fig. 10, top row) future snowfall furthermore occurs in a narrower temperature range (Fig. 10, second row).

Contrasting this general pattern of frequency-driven decreases of both mean and heavy snowfall, no changes or even slight increases of S_{mean}, S_{q99} and S_{1d} at high elevations are expected in mid-winter (see Fig. 8). This can to some part be explained by the general increase of total winter precipitation (Rajczak et al., 2017; Smiatek et al., 2016) that obviously offsets the warming effect in high-elevation regions where a substantial fraction of the future temperature PDF is still located below the rain-snow transition (Fig. 10, top row). This process has also been identified in previous works to be, at last partly, responsible for future snowfall increases (de Vries et al., 2014; Krasting et al., 2013; Räisänen, 2016). Furthermore, the magnitude of the increases of both mean and heavy snowfall is obviously driven by positive changes of S_{int}, while S_{freq} remains constant (Fig. 9c,g). An almost linear relationship between positive changes of S_{int} and positive changes of S_{mean} and S_{q99} is obtained (Fig. 9d,h; upper right quadrants. Nevertheless, the high-elevation mid-winter growth in S_{mean} is smaller than the identified increases of mean winter total precipitation. This can be explained by the persistent decrease of S_{frac} during the cold season (see Fig. 8, lowermost row).

For elevation intervals with simulated monthly temperatures between -6°C and 0°C in the CTRL period, S_{mean} appears to decrease stronger than S_{q99} (cf. Fig. 9b,f). O'Gorman (2014) found a very similar behaviour when analysing mean and extreme snowfall projections over the Northern Hemisphere within a set of GCMs. This finding is related to the fact that future snowfall decreases are mainly governed by a decrease of snowfall frequency while snowfall increases in high-elevated regions in mid-winter seem to be caused by increases of snowfall intensity. It can obviously be explained by the insensitivity of the temperature interval at which extreme snowfall occurs to climate warming and by the shape of the temperature – snowfall intensity distribution itself (Fig. 10, third row). The likely reason behind positive changes of S_{int} at high-elevated and cold regions is the higher water holding capacity of the atmosphere in a warmer climate. According to the Clausius-Clapeyron relation, saturation vapour pressure increases by about 7% per degree warming (Held and Soden, 2006). Previous studies have shown that simulated changes of heavy and extreme precipitation on daily time scales are consistent with this theory (e.g., Allen and Ingram, 2002; Rajczak et al., 2017). In terms of snowfall, we find the Clausius-Clapeyron relation to be applicable for negative temperatures up to approximately -5°C as well (Fig. 10, third row, dashed lines). Inconsistencies for temperatures between -5°C and 0°C are due to a snow fraction *sf* < 100% for corresponding precipitation events.

For further clarification, Figure 11 schematically illustrates the governing processes behind the changes of mean and heavy snowfall that differ between climatologically warm (decreasing snowfall) and climatologically cold climates (increasing snowfall). As shown in Figure 10 (third row), the mean S_{int} distribution is rather independent on future warming and similar temperatures are associated with similar mean snowfall intensities. In particular, heaviest snowfall is expected to occur slightly below the freezing level in both the CTRL and the SCEN period (Fig. 11a). How often do such conditions prevail in the two periods? In a warm current climate, i.e., at low elevations or in the transition seasons, heavy snowfall only rarely occurs as the temperature interval for highest snowfall intensity is already situated in the left tail of the CTRL period's temperature distribution (Fig. 11b). With future warming, i.e., with a shift of the temperature distribution to the right, the probability for days to occur in the heavy snowfall temperature interval (dark grey shading) decreases stronger than the probability of days to occur in the overall snowfall regime (light grey shading). This results in (1) a general decrease of snowfall frequency, (2) a general decrease of mean snowfall intensity and (3) a general and similar decrease of both mean and heavy snowfall amounts. In contrast, at cold and high-elevated sites CTRL period temperatures are often too low to trigger heavy snowfall since a substantial fraction of the temperature PDF is located to the left of the heavy snowfall temperature interval (Fig. 11 c). The shifted distribution in a warmer SCEN climate, however, peaks within the temperature interval that favours heavy snowfall. This leads to a probability increase for days to occur in the heavy snowfall temperature range despite the general reduction in S_{freq} (lower overall probability of days to occur in the entire snowfall regime, light grey). As a consequence, mean S_{int} tends to increase and the reduction of heavy snowfall amounts is less pronounced (or even of opposing sign) than the reduction in mean snowfall. For individual (climatologically cold) regions and seasons, the increase of mean S_{int} might even compensate the S_{freq} decrease, resulting in an increase of both mean and heavy snowfall amounts. Note that in a strict sense these explanations only hold in the case that the probability of snowfall to occur at a given temperature does not change considerably between the CTRL and the SCEN period.

684 This behaviour is approximately found (Fig. 10, bottom row), which presumably indicates only minor
685 contributions of large scale circulation changes and associated humidity changes on both the
686 temperature - snowfall frequency and the temperature - snowfall intensity relation.

5.2 Emission scenario uncertainty

688 The projections presented in the previous sections are based on the RCP8.5 emission scenario, but
689 will depend on the specific scenario considered. To assess this uncertainty we here compare the
690 RCM_{sep+ba} simulations for the previously shown RCP8.5 emission scenario against those assuming the
691 more moderate RCP4.5 scenario. As a general picture, the weaker RCP4.5 scenario is associated
692 with less pronounced changes of snowfall indices (Fig. 12). Differences in mean seasonal δS_{mean}
693 between the two emission scenarios are most pronounced below 1000 m a.s.l. where percentage
694 changes for RCP4.5 are about one third smaller than for RCP8.5. At higher elevations, multi-model
695 mean changes better agree and the multi-model ranges for the two emission scenarios start
696 overlapping, i.e., individual RCP4.5 experiments can be located in the RCP8.5 multi-model range and
697 vice versa. Over the entire Alpine domain, about -25% of current snowfall is expected to be lost under
698 the moderate RCP4.5 emission scenario while a reduction of approximately -45% is projected for
699 RCP8.5. For seasonal cycles, the difference of δS_{mean} between RCP4.5 and RCP8.5 is similar for
700 most months and slightly decreases with altitude. Above 2000 m a.s.l., the simulated increase of S_{mean}
701 appears to be independent of the chosen RCP in January and February, while negative changes
702 before and after mid-winter are more pronounced for RCP8.5. Alpine domain mean δS_{q99} almost
703 doubles under the assumption of stronger GHG emissions. This is mainly due to differences at low
704 elevations whereas above 2000 m a.s.l. δS_{q99} does not seem to be strongly affected by the choice of
705 the emission scenario. Differences in monthly mean changes are in close analogy to δS_{mean}. Higher
706 emissions lead to a further negative shift in δS_{q99}. Up to mid-elevations differences are rather
707 independent of the season. However, at highest elevations and from January to March, differences
708 between RCP4.5 and RCP8.5 are very small.

709 Despite the close agreement of mid-winter snowfall increases at high elevations between the two
710 emission scenarios, obvious differences in the spatial extent of the region of mean seasonal snowfall
711 increases can be found (cf Figs. S7 and 7 for δS_{mean}, and Figs. S8 and S9 for δS_{q99}). In most
712 simulations, the number of grid cells along the main Alpine ridge that show either little change or even
713 increases of seasonal mean S_{mean} or S_{q99} is larger for RCP4.5 than for RCP8.5 with its larger warming
714 magnitude.

5.3 Intercomparison of projections with separated and raw snowfall

716 The snowfall projections presented above are based on the RCM_{sep+ba} data set, i.e. on separated and
717 bias-adjusted snowfall amounts. To assess the robustness of these estimates we here compare the
718 obtained change signals against the respective signals based on $RCM_{sep+nba}$ (separated and not bias-
719 adjusted) and simulated raw snowfall output (RCM_{raw}). This comparison is restricted to the seven
720 RCMs providing raw snowfall as output variable (see Tab. 1).

721 The three different change estimates agree well with each other in terms of relative snowfall change
722 signals (Fig. 13, top row). Multi-model mean relative changes are very similar for all analysed snowfall
723 indices and elevation intervals. In many cases, separated and not bias-adjusted snowfall ($RCM_{sep+nba}$)
724 is subject to slightly smaller percentage decreases. Multi-model mean differences between RCM_{sep+ba},
725 $RCM_{sep+nba}$ and RCM_{raw} simulations are smaller than the corresponding multi-model spread of
726 RCM_{sep+ba} simulations and emission scenario uncertainties (cf. Figs. 12, 13 and S10). This agreement
727 in terms of relative change signals is in contrast to absolute change characteristics (Fig. 13, bottom
728 row). Results based on the three data sets agree in the sign of change, but not in their magnitude,
729 especially at high elevations >2000 m a.s.l.. As the relative changes are almost identical, the absolute
730 changes strongly depend upon the treatment of biases in the control climate.

731 In summary, these findings indicate that (a) the snowfall separation method developed in the present
732 work yields rather good proxies for relative changes of snowfall indices in raw RCM output (which is
733 not available for all GCM-RCM chains), and that (b) the additional bias adjustment of separated
734 snowfall amounts only has a weak influence on relative change signals of snowfall indices, but can
735 have substantial effects on absolute changes.

6 Conclusions and outlook

737 The present work makes use of state-of-the-art EURO-CORDEX RCM simulations to assess changes
738 of snowfall indices over the European Alps by the end of the 21st century. For this purpose, snowfall is
739 separated from total precipitation using near-surface air temperature in both the RCMs and in the
740 observation-based estimate on a daily basis. The analysis yields a number of robust signals,
741 consistent across a range of climate model chains and across emission scenarios. Relating to the
742 main objectives we find the following:

743 **Snowfall separation on the RCM grid.** Binary snow fractionation with a fixed temperature threshold
744 on coarse-resolution grids (with 11 km resolution) leads to an underestimation of mean snowfall and
745 an overestimation of heavy snowfall. To overcome these deficiencies, the Richards snow fractionation
746 method is implemented. This approach expresses that the coarse-grid snow fraction depends not only
747 on daily mean temperature, but also on topographical subgrid-scale variations. Accounting for the
748 latter results in better estimates for mean and heavy snowfall. However, due to limited observational
749 coverage the parameters of this method are fitted for Switzerland only and are then applied to the
750 entire Alpine domain. Whether this spatial transfer is robust could further be investigated by using
751 observational data sets covering the full domain of interest but is out of the scope of this study.

752 **Snowfall bias adjustment.** Simulations of the current EURO-CORDEX ensemble are subject to
753 considerable biases in precipitation and temperature, which translate into biased snowfall amounts. In
754 the EVAL period, simulated precipitation is largely overestimated, with increasing biases toward higher
755 altitudes. On the other hand, simulated near surface temperatures are generally too low with largest
756 deviations over mountainous regions. These findings were already reported in previous studies for
757 both the current EURO-CORDEX data set but also for previous RCM ensembles (e.g. Frei et al., 2003;
758 Kotlarski et al., 2012; Kotlarski et al., 2015; Rajczak et al., 2013; Smiatek et al., 2016). By

implementing a simple bias adjustment approach, we are able to partly reduce these biases and the associated model spread, which should enable more robust change estimates. The adjusted model results reproduce the seasonal cycles of mean snowfall fairly well. However, substantial biases remain in terms of heavy snowfall, snowfall intensities (which in general are overestimated), snowfall frequencies, and spatial snowfall distributions. Further improvements might be feasible by using more sophisticated bias adjustment methods, such as quantile mapping (e.g., Rajczak et al., 2016), local intensity scaling of precipitation (e.g., Schmidli et al., 2006), or weather generators (e.g. Keller at al., 2016). Advantages of the approach employed here are its simplicity, its direct linkage to the snowfall separation method and, as a consequence, its potential ability to account for non-stationary snowfall biases. Furthermore, a comparison to simulated raw snowfall for a subset of seven simulations revealed that relative change signals are almost independent of the chosen post-processing strategy.

Snowfall projections for the late 21st century. Snowfall climate change signals are assessed by deriving the changes in snowfall indices between the CTRL period 1981 - 2010 and the SCEN period 2070 - 2099. Our results show that by the end of the 21st century, snowfall over the Alps will be considerably reduced. Between September and May mean snowfall is expected to decrease by approximately -45% (multi-model mean) under an RCP8.5 emission scenario. For the more moderate RCP4.5 scenario, multi-model mean projections show a decline of -25%. These results are in good agreement with previous works (e.g. de Vries et al., 2014; Piazza et al., 2014, Räisänen, 2016). Low-lying areas experience the largest percentage changes of more than -80%, while the highest Alpine regions are only weakly affected. Variations of heavy snowfall, defined by the 99% all-day snowfall percentile, show an even more pronounced signal at low-lying elevations. With increasing elevation, percentage changes of heavy snowfall are generally smaller than for mean snowfall. O'Gorman (2014) found a very similar behaviour by analysing projected changes in mean and extreme snowfall over the entire Northern Hemisphere. He pointed out that heavy and extreme snowfall occurs near an optimal temperature (near or below freezing, but not too cold), which seems to be independent of climate warming. We here confirm this finding. At mid and high elevations heavy snowfall in a warmer climate will still occur in the optimal temperature range, hence, heavy snowfall amounts will decrease less strongly compared to mean snowfall, and may even increase in some areas.

At first approximation, the magnitude of future warming strongly influences the reduction of mean and heavy snowfall by modifying the snowfall frequency. Snowfall increases may however occur at high (and thus cold) elevations, and these are not caused by frequency changes. Here, snowfall increases due to (a) a general increase of total winter precipitation combined with only minor changes in snowfall frequency, and (b) more intense snowfall. This effect has a pronounced altitudinal distribution and may be particularly strong under conditions (depending upon location and season) where the current climate is well below freezing. With the expected warming a shift towards a temperature range more favourable to snowfall (near or below freezing, but not too cold) can be expected with corresponding increases of mean snowfall, despite a general decrease of the snowfall fraction.

Note that individual EURO-CORDEX experiments were completely or partly omitted from our analysis (see Supplementary Material, Part B and Table 1). However, when comparing the ensemble results

based on the reduced and the full model set only slight differences are found and our main results and conclusions do not change (compare Figure 12 to Figure S15). This indicates a robust ensemble analysis that is only little affected by potentially critical shortcomings of individual simulations.

The identified future changes of snowfall over the Alps can lead to a variety of impacts in different sectors. With decreasing snowfall frequencies and the general increase of the snowline (e.g., Beniston, 2003; Gobiet et al., 2014; Hantel et al., 2012), both associated with temperature changes, ski lift operators are looking into an uncertain future. A shorter snowfall season will likely put them under greater financial pressure. Climate change effects might be manageable only for ski areas reaching up to high elevations (e.g. Elsasser and Bürki, 2002). Even so these resorts might start later into the ski season, the snow conditions into early spring could change less dramatically due to projected high-elevation snowfall increases in mid-winter. A positive aspect of the projected decrease in snowfall frequency might be a reduced expenditures for airport and road safety (e.g., Zubler et al., 2015).

At lower altitudes, an intensification of winter precipitation, combined with smaller snowfall fractions (Serquet et al., 2013), increases the flood potential (Beniston, 2012). Snow can act as a buffer by releasing melt water constantly over a longer period of time. With climate warming, this storage capacity is lost, and heavy precipitation immediately drains into streams and rivers which might not be able to take up the vast amount of water fast enough. Less snowmelt will also have impacts on hydropower generation and water management (e.g., Weingartner et al., 2013). So far, many Alpine regions are able to bypass dry periods by tapping melt water from mountainous regions. With reduced snow-packs due to less snowfall, water shortage might become a serious problem in some areas.

Regarding specific socio-economic impacts caused by extreme snowfall events, conclusions based on the results presented in this study are difficult to draw. It might be possible that the 99% all-day snowfall percentile we used for defining heavy snowfalls, is not appropriate to speculate about future evolutions of (very) rare events (Schär et al., 2016). To do so, one might consider applying a generalized extreme value (GEV) analysis which is more suitable for answering questions related to rare extreme events.

7 Data Availability

The EURO-CORDEX RCM data analysed in the present work are publicly available - parts of them for non-commercial use only - via the Earth System Grid Federation archive (ESGF; e.g., https://esgf-data.dkrz.de). The observational datasets RHiresD and TabsD as well as the snow depth data for Switzerland are available for research and educational purposes from kundendienst@meteoschweiz.ch. The analysis code is available from the corresponding author on request.

8 Competing Interests

The authors declare that they have no conflict of interest.

9 Acknowledgements

We gratefully acknowledge the support of Jan Rajczak, Urs Beyerle and Curdin Spirig (ETH Zurich) as well as Elias Zubler (MeteoSwiss) in data acquisition and pre-processing. Christoph Frei (MeteoSwiss) and Christoph Marty (WSL-SLF) provided important input on specific aspects of the analysis. The GTOPO30 digital elevation model is available from the U.S. Geological Survey. Finally, we thank the climate modelling groups of the EURO-CORDEX initiative for producing and making available their model output.

10 References

Abegg, B. A., S., Crick, F., and de Montfalcon, A.: Climate change impacts and adaptation in winter tourism, in: Climate change in the European Alps: adapting winter tourism and natural hazards management, edited by: Agrawala, S., Organisation for Economic Cooperation and Development (OECD), Paris, France, 25-125, 2007.

Allen, M. R., and Ingram, W. J.: Constraints on future changes in climate and the hydrologic cycle, Nature, 419, 224-232, 10.1038/nature01092, 2002.

Beniston, M.: Climatic Change in Mountain Regions: A Review of Possible Impacts. Clim Change, 59, 5-31.

Beniston, M.: Impacts of climatic change on water and associated economic activities in the Swiss Alps, J Hydrol, 412, 291-296, 10.1016/j.jhydrol.2010.06.046, 2012.

Ceppi, P., Scherrer, S.C., Fischer, A.M., and Appenzeller, C.: Revisiting Swiss temperature trends 1959–2008, Int J Climatol, 32, 203-213, 10.1002/joc.2260, 2012.

CH2011: Swiss Climate Change Scenarios CH2011, published by C2SM, MeteoSwiss, ETH, NCCR Climate, and OcCC, Zurich, Switzerland, 88 pp, 2011.

Chimani, B., Böhm, R., Matulla, C., and Ganekind, M.: Development of a longterm dataset of solid/liquid precipitation, Adv Sci Res, 6, 39-43, 10.5194/asr-6-39-2011, 2011.

de Vries, H., Haarsma, R. J., Hazeleger, W.: On the future reduction of snowfall in western and central Europe. Clim Dyn, 41, 2319-2330, 10.1007/s00382-012-1583-x, 2013.

de Vries, H., Lenderink, G., and van Meijgaard, E.: Future snowfall in western and central Europe projected with a high-resolution regional climate model ensemble, Geophys Res Lett, 41, 4294-4299, 10.1002/2014GL059724, 2014.

Deser, C., Knutti, R., Solomon, S. and Phillips, A. S.: Communication of the role of natural variability in future North American climate. Nature Clim Change, 2, 775-779, 2012.

Elsasser, H. and Bürki, R.: Climate change as a threat to tourism in the Alps. Climate Research, 20, 253-257.

864 Fischer, A. M., Keller, D. E., Liniger, M. A., Rajczak, J., Schär, C., and Appenzeller, C.: Projected changes in
865 precipitation intensity and frequency in Switzerland: a multi-model perspective, Int J Climatol, 35, 3204-3219,
866 10.1002/joc.4162, 2015.

867 Fischer, E. M. and Knutti, R.: Observed heavy precipitation increase confirms theory and early models. Nature
868 Clim Change, 6, 986-992, 10.1038/NCLIMATE3110, 2016.

869 Frei, C. and Schär, C.: A precipitation climatology of the Alps from high-resolution rain-gauge observations, Int J
870 Climatol, 18, 873-900, 10.1002/(Sici)1097-0088(19980630)18:8<873::Aid-Joc255>3.0.Co;2-9, 1998.

871 Frei, C., Christensen, J. H., Déqué, M., Jacob, D., Jones, R. G., and Vidale, P. L.: Daily precipitation statistics in
872 regional climate models: Evaluation and intercomparison for the European Alps, J Geophys Res-Atmos, 108,
873 10.1029/2002jd002287, 2003.

874 Frei, C.: Interpolation of temperature in a mountainous region using nonlinear profiles and non-Euclidean
875 distances, Int J Climatol, 34, 1585-1605, 10.1002/joc.3786, 2014.

876 Giorgi, F.: Simulation of regional climate using a limited area model nested in a general circulation model, J
877 Climate, 3, 941-963, 1990.

878 Giorgi, F., Jones, C., and Asrar, G. R.: Addressing climate information needs at the regional level: the CORDEX
879 framework, World Meteorological Organization (WMO) Bulletin, 58, 175, 2009.

880 Giorgi, F., Torma, C., Coppola, E., Ban, N., Schär, C., and Somot, S.: Enhanced summer convective rainfall at
881 Alpine high elevations in response to climate warming, Nat Geo, 9, 584-589, 10.1038/ngeo2761, 2016.

882 Gobiet, A., Kotlarski, S., Beniston, M., Heinrich, G., Rajczak, J., and Stoffel, M.: 21st century climate change in
883 the European Alps - A review, Science of the Total Environment, 493, 1138-1151,
884 10.1016/j.scitotenv.2013.07.050, 2014.

885 Grünewald, T., and Lehning, M.: Are flat-field snow depth measurements representative? A comparison of
886 selected index sites with areal snow depth measurements at the small catchment scale, Hydrol Processes, 29,
887 1717-1728, 10.1002/hyp.10295, 2015.

888 Hantel, M., Maurer, C., and Mayer, D.: The snowline climate of the Alps 1961–2010. Theor Appl Climatol, 110,
889 517, 10.1007/s00704-012-0688-9, 2012.

890 Hawkins, E., and Sutton, R.: The Potential to Narrow Uncertainty in Regional Climate Predictions, B Am Meteorol
891 Soc, 90, 1095-+, 10.1175/2009BAMS2607.1, 2009.

892 Haylock, M.R., Hofstra, N., Klein Tank, A.M.G., Klok, E.J., Jones, P.D., and New, M.: A European daily high-
893 resolution gridded data set of surface temperature and precipitation for 1950–2006, J Geophys Res, 113,
894 D20119, 10.1029/2008JD010201.

895 Held, I. M., and Soden, B. J.: Robust responses of the hydrological cycle to global warming, J Climate, 19, 5686-
896 5699, 10.1175/Jcli3990.1, 2006.

897 IPCC: Climate Change 2013: The Physical Science Basis. Contribution of Working Group I to the Fifth
898 Assessment Report of the Intergovernmental Panel on Climate Change, Cambridge University Press, Cambridge,
899 United Kingdom and New York, NY, USA, 1535 pp., 2013.

900 Isotta, F. A., Frei, C., Weilguni, V., Tadic, M. P., Lassegues, P., Rudolf, B., Pavan, V., Cacciamani, C., Antolini,
901 G., Ratto, S. M., Munari, M., Micheletti, S., Bonati, V., Lussana, C., Ronchi, C., Panettieri, E., Marigo, G., and
902 Vertacnik, G.: The climate of daily precipitation in the Alps: development and analysis of a high-resolution grid
903 dataset from pan-Alpine rain-gauge data, Int J Climatol, 34, 1657-1675, 10.1002/joc.3794, 2014.

904 Jacob, D., Petersen, J., Eggert, B., Alias, A., Christensen, O. B., Bouwer, L. M., Braun, A., Colette, A., Déqué, M.,
905 Georgievski, G., Georgopoulou, E., Gobiet, A., Menut, L., Nikulin, G., Haensler, A., Hempelmann, N., Jones, C.,
906 Keuler, K., Kovats, S., Kröner, N., Kotlarski, S., Kriegsmann, A., Martin, E., van Meijgaard, E., Moseley, C.,
907 Pfeifer, S., Preuschmann, S., Radermacher, C., Radtke, K., Rechid, D., Rounsevell, M., Samuelsson, P., Somot,
908 S., Soussana, J. F., Teichmann, C., Valentini, R., Vautard, R., Weber, B., and Yiou, P.: EURO-CORDEX: new
909 high-resolution climate change projections for European impact research, Reg Environ Change, 14, 563-578,
910 10.1007/s10113-013-0499-2, 2014.

911 Keller, D. E., Fischer, A. M., Liniger, M. A., Appenzeller, C. and Knutti, R.: Testing a weather generator for
912 downscaling climate change projections over Switzerland. Int J Climatol, doi:10.1002/joc.4750, 2016.

913 Kienzle, S. W.: A new temperature based method to separate rain and snow, Hydrol Process, 22, 5067-5085,
914 10.1002/hyp.7131, 2008.

915 Kotlarski, S., Bosshard, T., Lüthi, D., Pall, P., and Schär, C.: Elevation gradients of European climate change in
916 the regional climate model COSMO-CLM. Clim Change, 112, 189-215, 10.1007/s10584-011-0195-5, 2012.

917 Kotlarski, S., Keuler, K., Christensen, O. B., Colette, A., Deque, M., Gobiet, A., Goergen, K., Jacob, D., Luthi, D.,
918 van Meijgaard, E., Nikulin, G., Schar, C., Teichmann, C., Vautard, R., Warrach-Sagi, K., and Wulfmeyer, V.:
919 Regional climate modeling on European scales: a joint standard evaluation of the EURO-CORDEX RCM
920 ensemble, Geosci Model Dev, 7, 1297-1333, 10.5194/gmd-7-1297-2014, 2014.

921 Kotlarski, S., Lüthi, D., and Schär, C.: The elevation dependency of 21st century European climate change: an
922 RCM ensemble perspective, Int J Climatol, 35, 3902-3920, 10.1002/joc.4254, 2015.

923 Krasting, J. P., Broccoli, A. J., Dixon, K. W., and Lanzante, J. R.: Future Changes in Northern Hemisphere
924 Snowfall. J Clim, 26, 7813-7828, 10.1175/JCLI-D-12-00832.1, 2013.

925 Laternser, M., and Schneebeli, M.: Long-term snow climate trends of the Swiss Alps (1931-99), Int J Climatol, 23,
926 733-750, 10.1002/joc.912, 2003.

927 Marty, C.: Regime shift of snow days in Switzerland, Geophys Res Lett, 35, 10.1029/2008gl033998, 2008.

928 Marty, C., and Blanchet, J.: Long-term changes in annual maximum snow depth and snowfall in Switzerland
929 based on extreme value statistics, Clim Change, 111, 705-721, 2011.

930 McAfee, S. A., Walsh, J., and Rupp, T. S.: Statistically downscaled projections of snow/rain partitioning for
931 Alaska, Hydrol Process, 28, 3930-3946, 10.1002/hyp.9934, 2014.

932 MeteoSchweiz: Klimareport 2015. Bundesamt für Meteorologie und Klimatologie MeteoSchweiz, Zürich.

933 MeteoSwiss: Daily Precipitation (final analysis): RhiresD:
934 www.meteoswiss.admin.ch/content/dam/meteoswiss/de/service-und-publikationen/produkt/raeumliche-daten-
935 niederschlag/doc/ProdDoc_RhiresD.pdf, access: 10.01.2017, 2013a.

936 MeteoSwiss: Daily Mean, Minimum and Maximum Temperature: TabsD, TminD ,TmaxD:
937 www.meteoswiss.admin.ch/content/dam/meteoswiss/de/service-und-publikationen/produkt/raeumliche-daten-
938 temperatur/doc/ProdDoc_TabsD.pdf, access: 10.01.2017, 2013b.

939 Moss, R. H., Edmonds, J. A., Hibbard, K. A., Manning, M. R., Rose, S. K., van Vuuren, D. P., Carter, T. R., Emori,
940 S., Kainuma, M., Kram, T., Meehl, G. A., Mitchell, J. F. B., Nakicenovic, N., Riahi, K., Smith, S. J., Stouffer, R. J.,
941 Thomson, A. M., Weyant, J. P., and Wilbanks, T. J.: The next generation of scenarios for climate change research
942 and assessment, Nature, 463, 747-756, 10.1038/nature08823, 2010.

943 Neff, E. L.: How Much Rain Does a Rain Gauge Gauge, J Hydrol, 35, 213-220, 10.1016/0022-1694(77)90001-4,
944 1977.

945 O'Gorman, P. A.: Contrasting responses of mean and extreme snowfall to climate change, Nature, 512, 416-
946 U401, 10.1038/nature13625, 2014.

947 Piazza, M., Boé, J., Terray, L., Pagé, C., Sanchez-Gomez, E., and Déqué, M.: Projected 21st century snowfall
948 changes over the French Alps and related uncertainties, Clim Change, 122, 583-594, 10.1007/s10584-013-1017-
949 8, 2014.

950 Räisänen, J.: Twenty-first century changes in snowfall climate in Northern Europe in ENSEMBLES regional
951 climate models, Clim Dynam, 46, 339-353, 10.1007/s00382-015-2587-0, 2016.

952 Rajczak, J., Pall, P., and Schär, C.: Projections of extreme precipitation events in regional climate simulations for
953 Europe and the Alpine Region, J Geophys Res-Atmos, 118, 3610-3626, 10.1002/jgrd.50297, 2013.

954 Rajczak, J., Kotlarski, S., and Schär, C.: Does Quantile Mapping of Simulated Precipitation Correct for Biases in
955 Transition Probabilities and Spell Lengths?, J Climate, 29, 1605-1615, 10.1175/Jcli-D-15-0162.1, 2016.

956 Rajczak, J. and Schär, C.: Projections of future precipitation extremes over Europe: a multi-model assessment of
957 climate simulations. J Geophys Res Atmos, in press, 2017.

958 Richards, F. J.: A Flexible Growth Function for Empirical Use, J Exp Bot, 10, 290-300, 10.1093/Jxb/10.2.290,
959 1959.

960 Rummukainen, M.: State-of-the-art with regional climate models, Wiley Interdisciplinary Reviews-Climate Change,
961 1, 82-96, 10.1002/wcc.8, 2010.

962 Schär, C., Ban, N., Fischer, E. M., Rajczak, J., Schmidli, J., Frei, C., Giorgi, F., Karl, T. R., Kendon, E. J., Tank, A.
963 M. G. K., O'Gorman, P. A., Sillmann, J., Zhang, X. B., and Zwiers, F. W.: Percentile indices for assessing changes
964 in heavy precipitation events, Clim Change, 137, 201-216, 10.1007/s10584-016-1669-2, 2016.

965 Scherrer, S. C., Appenzeller, C., and Laternser, M.: Trends in Swiss Alpine snow days: The role of local- and
966 large-scale climate variability, Geophys Res Lett, 31, 10.1029/2004gl020255, 2004.

967 Schmidli, J., Frei, C., and Vidale, P. L.: Downscaling from GCM precipitation: A benchmark for dynamical and
968 statistical downscaling methods, Int J Climatol, 26, 679-689, 10.1002/joc.1287, 2006.

969 Schmucki, E., Marty, C., Fierz, C., and Lehning, M.: Simulations of 21st century snow response to climate change
970 in Switzerland from a set of RCMs, Int J Climatol, 35, 3262-3273, 10.1002/joc.4205, 2015a.

971 Schmucki, E., Marty, C., Fierz, C., Weingartner, R. and Lehning, M.: Impact of climate change in Switzerland on
972 socioeconomic snow indices, Theor Appl Climatol, in press, 10.1007/s00704-015-1676-7, 2015b.

973 Serquet, G., Marty, C., and Rebetez, M.: Monthly trends and the corresponding altitudinal shift in the
974 snowfall/precipitation day ratio, Theor Appl Climatol, 114, 437-444, 10.1007/s00704-013-0847-7, 2013.Sevruk, B.:

975 Der Niederschlag in der Schweiz, Geographisches Institut der Eidgenössischen Technischen Hochschule in
976 Zürich, Abteilung Hydrologie, Zurich, Switzerland, 1985.

977 SFOE, Hydropower: http://www.bfe.admin.ch/themen/00490/00491/index.html?lang=en, access: 16.09.2016,
978 2014.

979 Smiatek, G., Kunstmann, H., and Senatore, A.: EURO-CORDEX regional climate model analysis for the Greater
980 Alpine Region: Performance and expected future change, J Geophys Res-Atmos, 121, 7710-7728,
981 10.1002/2015JD024727, 2016.

982 Soncini, A., and Bocchiola, D.: Assessment of future snowfall regimes within the Italian Alps using general
983 circulation models, Cold Reg Sci Technol, 68, 113-123, 10.1016/j.coldregions.2011.06.011, 2011.

984 Steger, C., Kotlarski, S., Jonas, T., and Schär, C.: Alpine snow cover in a changing climate: a regional climate
985 model perspective, Clim Dynam, 41, 735-754, 10.1007/s00382-012-1545-3, 2013.

986 Techel, F., Stucki, T., Margreth, S., Marty, C., and Winkler, K.: Schnee und Lawinen in den Schweizer Alpen.
987 Hydrologisches Jahr 2013/14, WSL-Institut für Schnee- und Lawinenforschung SLF, Birmensdorf, Switzerland,
988 2015.

989 Terzago, S., von Hardenberg, J., Palazzi, E., and Provenzale, A.: Snow water equivalent in the Alps as seen by
990 gridded datasets, CMIP5 and CORDEX climate models. The Cryosphere Discussion, 10.5194/tc-2016-280, 2017.

991 Torma, C., Giorgi, F., and Coppola, E.: Added value of regional climate modeling over areas characterized by
992 complex terrain Precipitation over the Alps, J Geophys Res-Atmos, 120, 3957-3972, 10.1002/2014JD022781,
993 2015.

994 Vautard, R., Gobiet, A., Jacob, D., Belda, M., Colette, A., Déqué, M., Fernandez, J., Garcia-Diez, M., Goergen,
995 K., Guttler, I., Halenka, T., Karacostas, T., Katragkou, E., Keuler, K., Kotlarski, S., Mayer, S., van Meijgaard, E.,
996 Nikulin, G., Patarcic, M., Scinocca, J., Sobolowski, S., Suklitsch, M., Teichmann, C., Warrach-Sagi, K.,
997 Wulfmeyer, V., and Yiou, P.: The simulation of European heat waves from an ensemble of regional climate
998 models within the EURO-CORDEX project, Clim Dynam, 41, 2555-2575, 10.1007/s00382-013-1714-z, 2013.

999 Weingartner, R., Schädler, B., and Hänggi, P.: Auswirkungen der Klimaänderung auf die schweizerische
1000 Wasserkraftnutzung, Geographica Helvetica, 68, 239-248, 2013.

1001 Yang, D. Q., Elomaa, E., Tuominen, A., Aaltonen, A., Goodison, B., Gunther, T., Golubev, V., Sevruk, B.,
1002 Madsen, H., and Milkovic, J.: Wind-induced precipitation undercatch of the Hellmann gauges, Nord Hydrol, 30,
1003 57-80, 1999.

1004 Zubler, E. M., Scherrer, S. C., Croci-Maspoli, M., Liniger, M. A., and Appenzeller, C.: Key climate indices in
1005 Switzerland; expected changes in a future climate, Clim Change, 123, 255-271, 10.1007/s10584-013-1041-8,
1006 2014.

1007 Zubler, E. M., Fischer, A. M., Liniger, M. A., and Schlegel, T.: Auftausalzverbrauch im Klimawandel, MeteoSwiss,
1008 Zurich, Switzerland, Fachbericht 253, 2015.

1009

1010 **Figures**

1011

1012
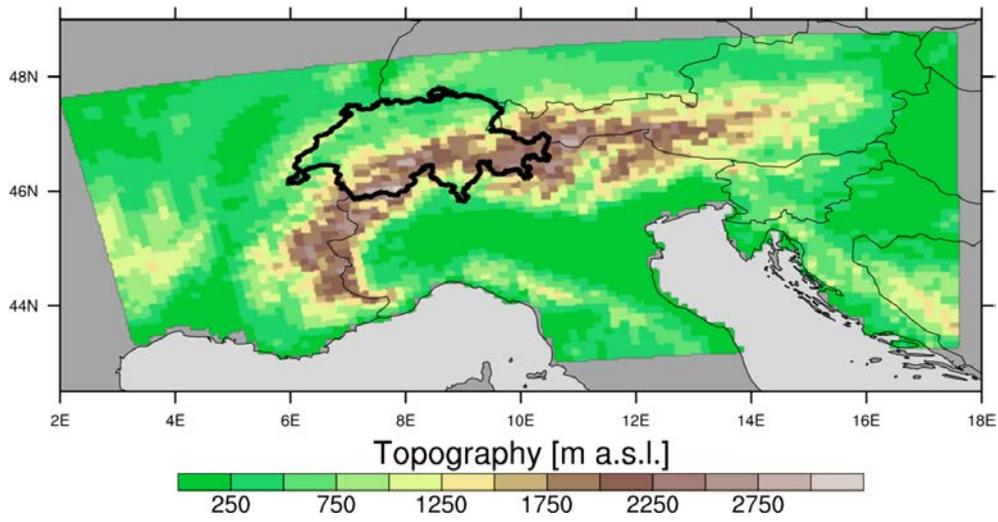
1013

1014

1015 **Figure 1** GTOPO30 topography (*https://lta.cr.usgs.gov/GTOPO30*) aggregated to the EUR-11 (0.11°) RCM grid.
1016 The coloured area shows the Alpine domain used for the assessment of snowfall projections. The bold black
1017 outline marks the Swiss sub-domain used for the assessment of the bias adjustment approach.

1018
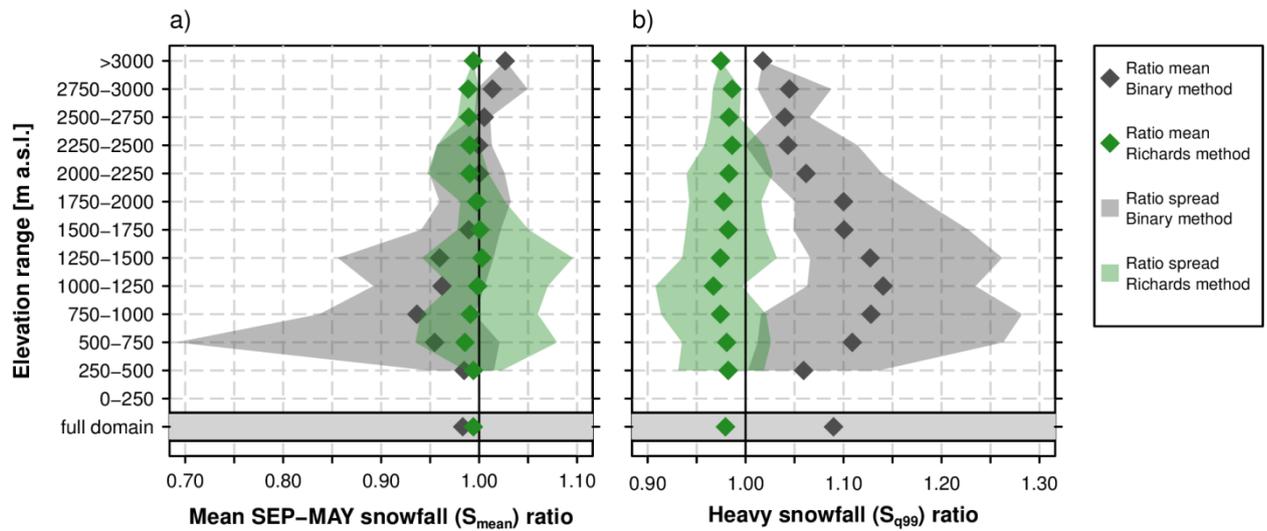
1019

1020

1021 **Figure 2** Snowfall ratios for the Binary and Richards snow fractionation method. Ratios represent the quotient of
1022 the snowfall as estimated by the respective method and the snowfall as estimated by the *Subgrid* method. Ratios
1023 are valid at the coarse-resolution grid (12 km). a) Ratios for mean snowfall, S_{mean}. b) Ratios for heavy snowfall,
1024 S_{q99}. Ratio means were derived after averaging the corresponding snowfall index for 250 m elevation intervals in
1025 Switzerland while the ratio spread represents the minimum and maximum grid point-based ratios in the
1026 corresponding elevation interval. This analysis is entirely based on the observational data sets TabsD and
1027 RhiresD.

1028
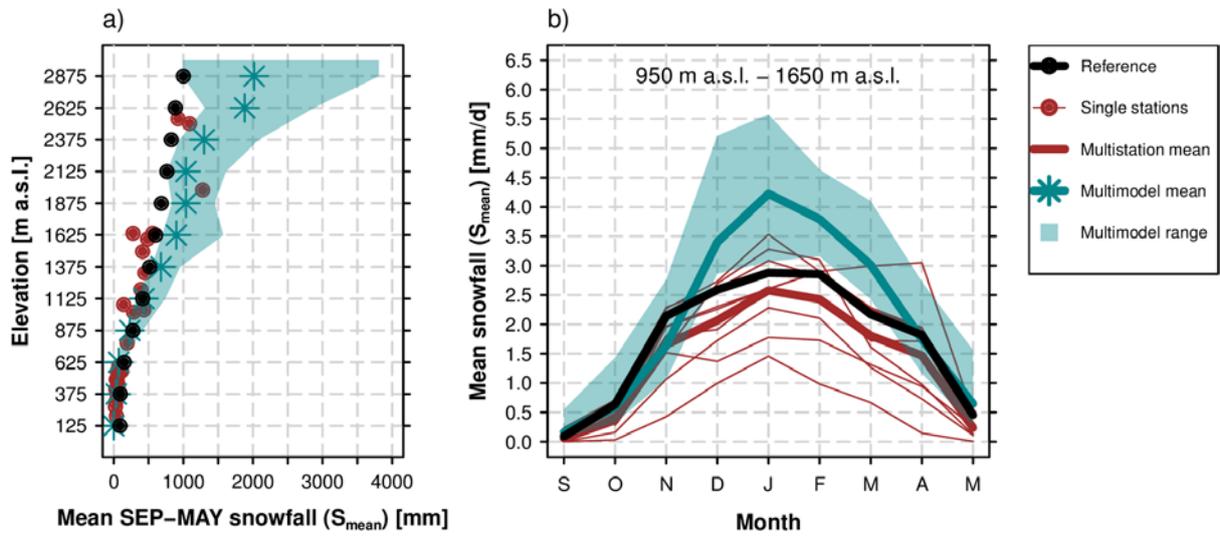
Figure 3 Comparison of measured fresh snow sums of 29 MeteoSwiss stations (red) against simulated RCM raw snowfall in Switzerland (green) and against the 2 km reference snowfall grid obtained by employing the *Subgrid method* (black) in the EVAL period 1971-2005. a) Mean September – May snowfall vs. elevation. Both the simulation data (green) and the reference data (black) are based on the spatio-temporal mean of 250 m elevation ranges and plotted at the mean elevation of the corresponding interval. b) Seasonal September-May snowfall cycle for the elevation interval 950 m a.s.l. to 1650 m a.s.l.. Simulated multi-model means and spreads are based on a subset of seven EURO-CORDEX simulations of the reduced model set providing raw snowfall as output variable (see Tab. 1).
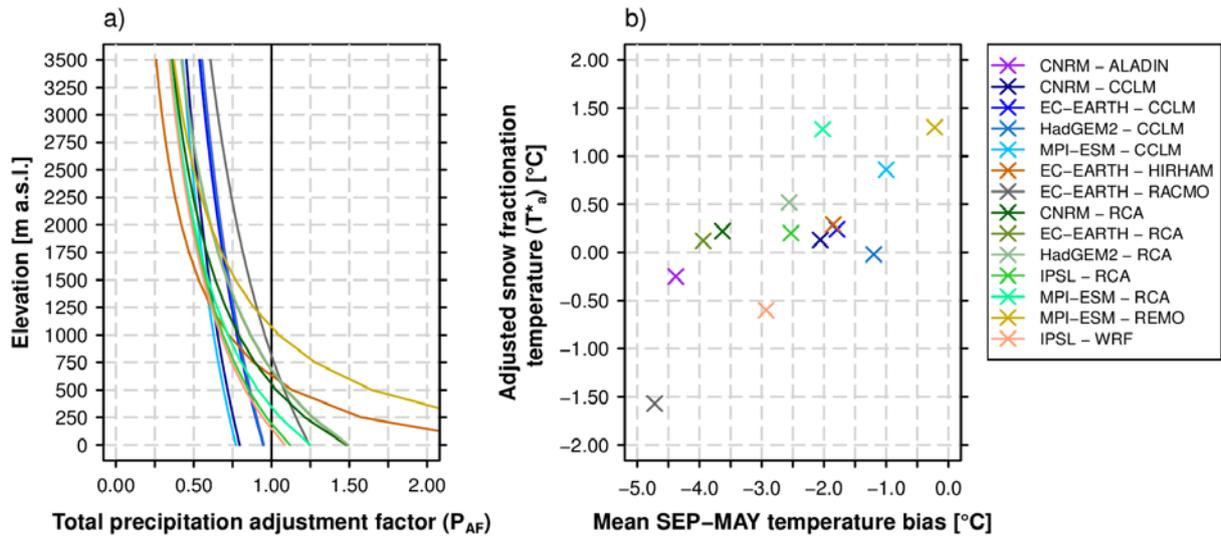
Figure 4 Overview of bias adjustment. a) Elevation-dependent total precipitation adjustment factors, P_{AF}, for the full model set (14 GCM-RCM chains; see Eq. 10). b) Scatterplot of mean September to May temperature biases (RCM simulation minus observational analysis) vs. adjusted snow fractionation temperatures, T^*_a.
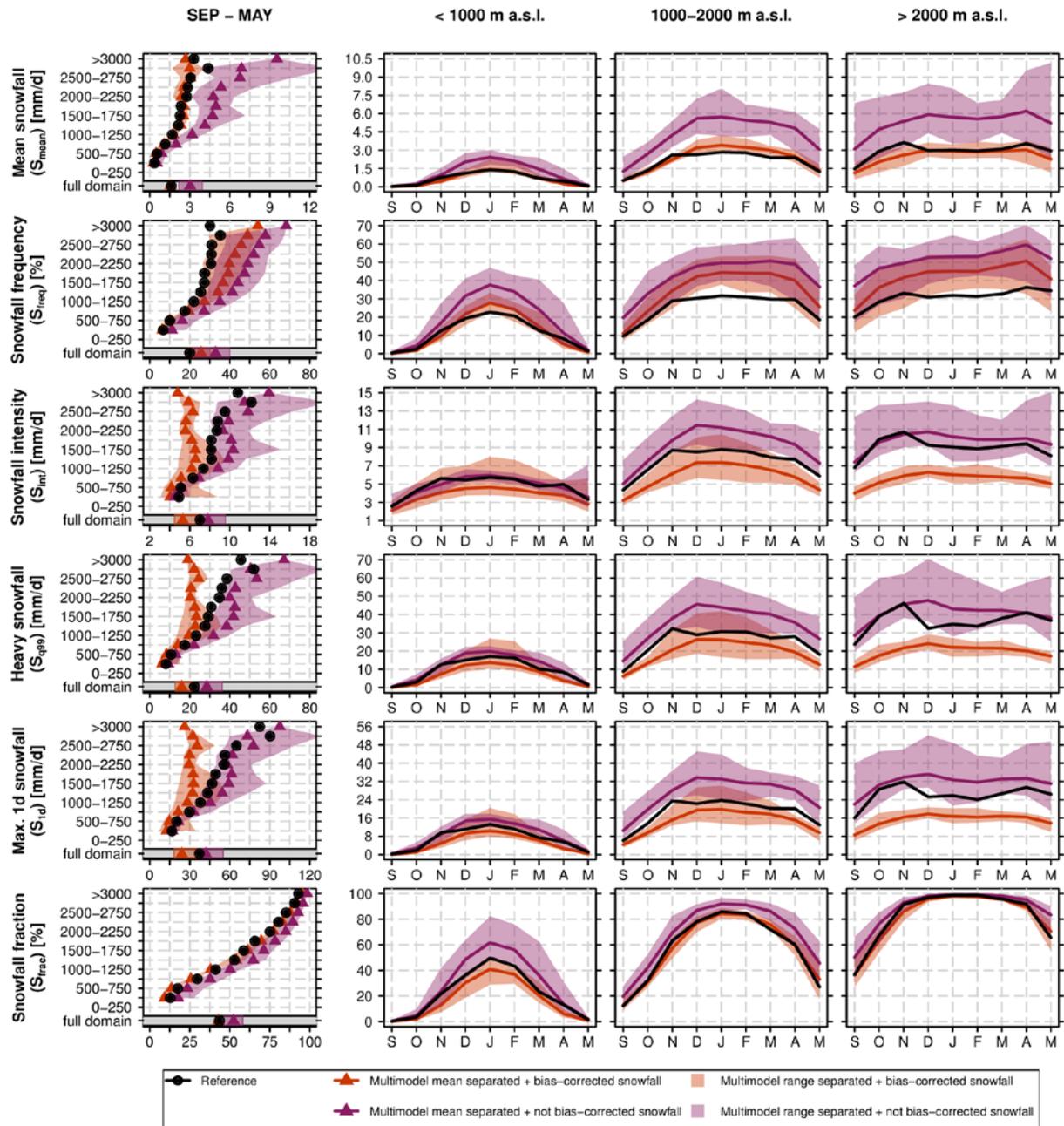
Figure 5 Evaluation of snowfall indices in the EVAL period 1971-2005 for the 12 snowfall separated + bias-adjusted (RCM$_{sep+ba}$) and 12 snowfall separated + not bias-adjusted (RCM$_{sep+nba}$) RCM simulations of the reduced model set vs. observation-based reference. The first column shows the mean September-May snowfall index statistics vs. elevation while the monthly snowfall indices (spatially averaged over the elevation intervals <1000 m.a.s.l., 1000 m a.s.l.-2000 m a.s.l. and >2000 m a.s.l.) are displayed in columns 2-4.
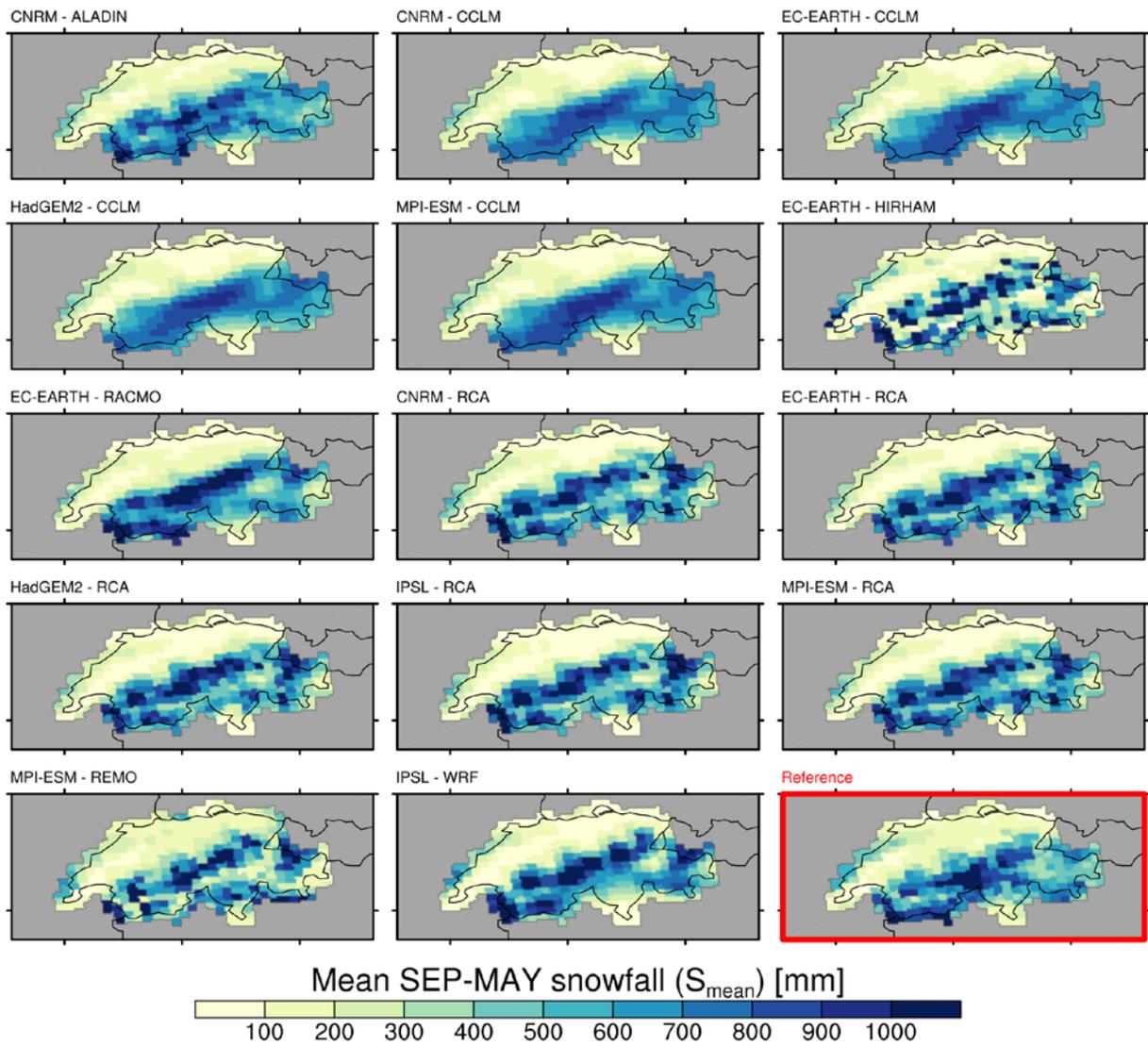
Figure 6 Spatial distribution of mean September-May snowfall, S_{mean}, in the EVAL period 1971-2005 and for the 14 snowfall separated + bias-adjusted RCM simulations (RCM_{sep+ba}) of the full model set. Lower right panel: observation-based reference.
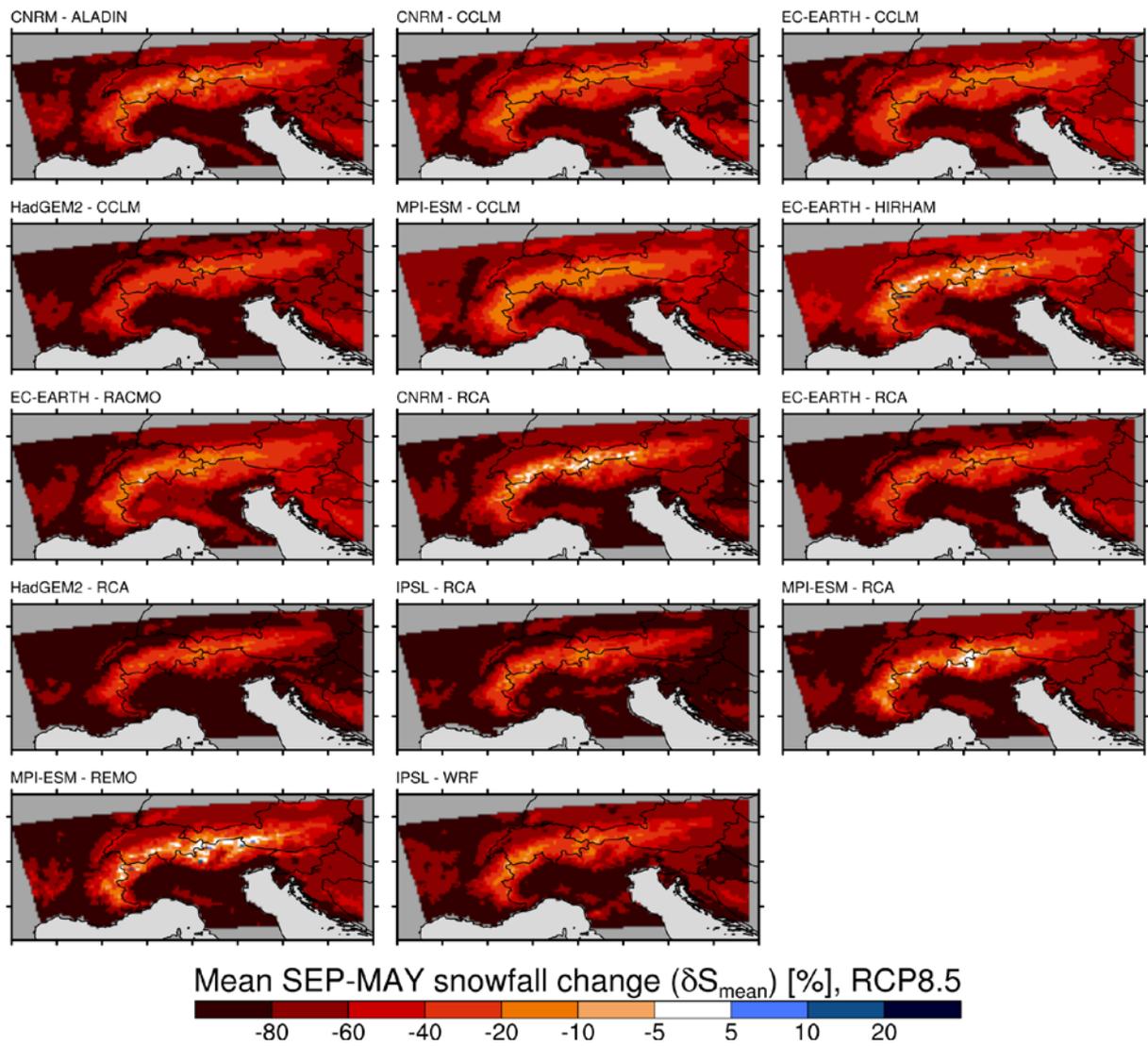
Figure 7 Spatial distribution of relative changes (SCEN period 2070-2099 with respect to CTRL period 1981-2010) in mean September-May snowfall, δS_{mean}, for RCP8.5 and for the 14 snowfall separated + bias-adjusted RCM simulations (RCM_{sep+ba}) of the full model set. For RCP4.5, see Fig. S7.

1064
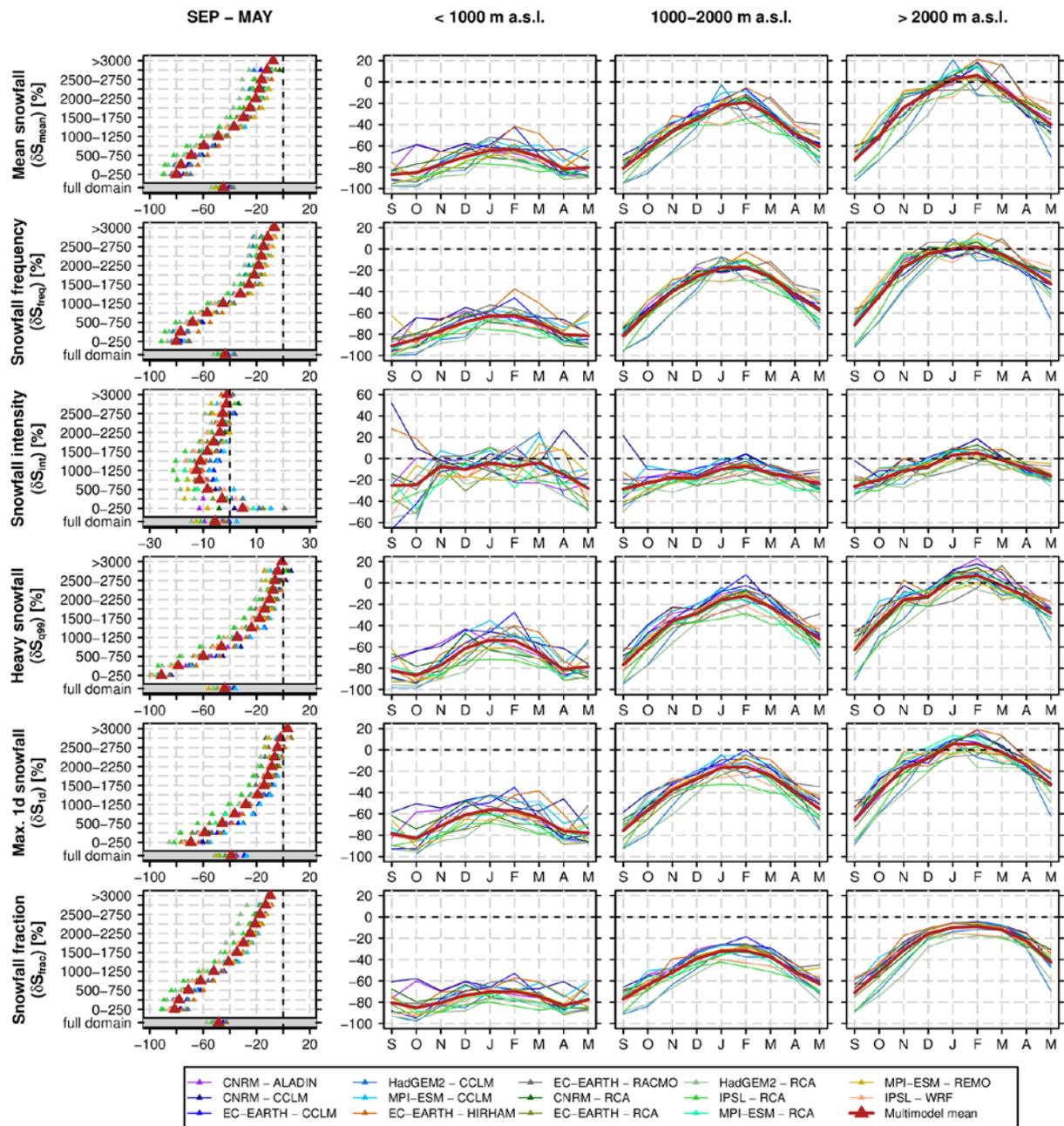
1065

Figure 8 Relative changes (SCEN period 2070-2099 with respect to CTRL period 1981-2010) of snowfall indices based on the 14 snowfall separated + bias-adjusted RCM simulations (RCM_{sep+ba}) of the full model set for RCP8.5. The first column shows the mean September-May snowfall index statistics vs. elevation. Monthly snowfall index changes (spatially averaged over the elevation intervals <1000 m.a.s.l., 1000 m a.s.l.-2000 m a.s.l. and >2000 m a.s.l.) are displayed in columns 2-4.

1071
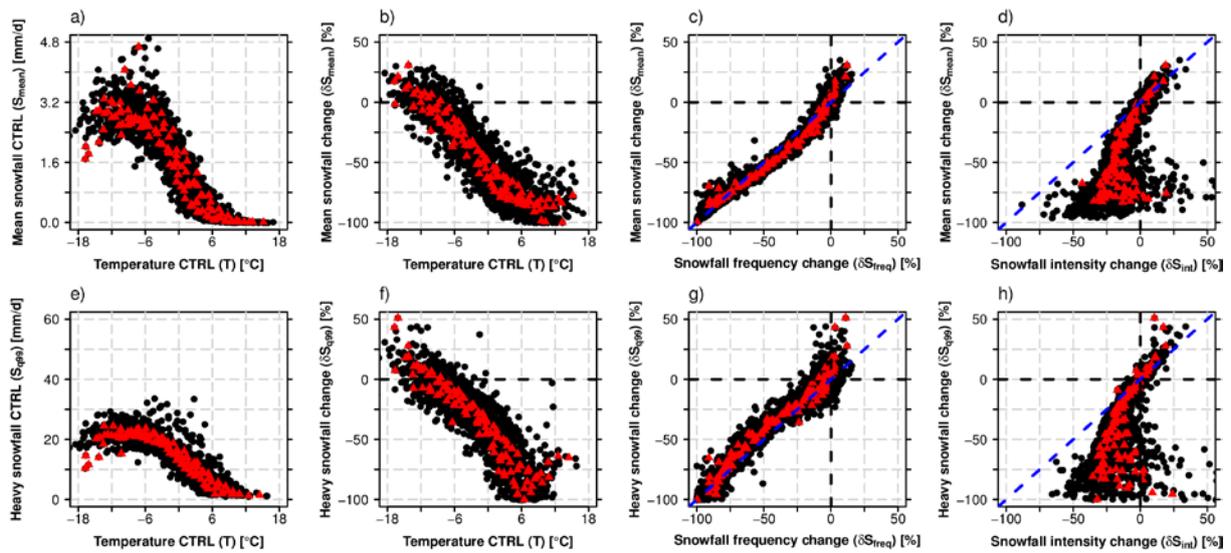
1072

1073

1074 **Figure 9** Intercomparison of various snowfall indices and relationship with monthly mean temperature in CTRL.
1075 For each panel, the monthly mean statistics for each 250 m elevation interval and for each of the 12 snowfall
1076 separated + bias-adjusted (RCMsep+ba) RCM simulations of the reduced model set (RCM$_{sep+ba}$) were derived
1077 (black circles). Red triangles denote the multi-model mean for a specific month and elevation interval. The
1078 monthly statistics were calculated by considering all grid points of the specific elevation intervals which are
1079 available for both variables in the corresponding scatterplot only (area consistency). Relative changes are based
1080 on the RCP8.5 driven simulations (SCEN 2070-2099 wrt. CTRL 1981-2010).

1081
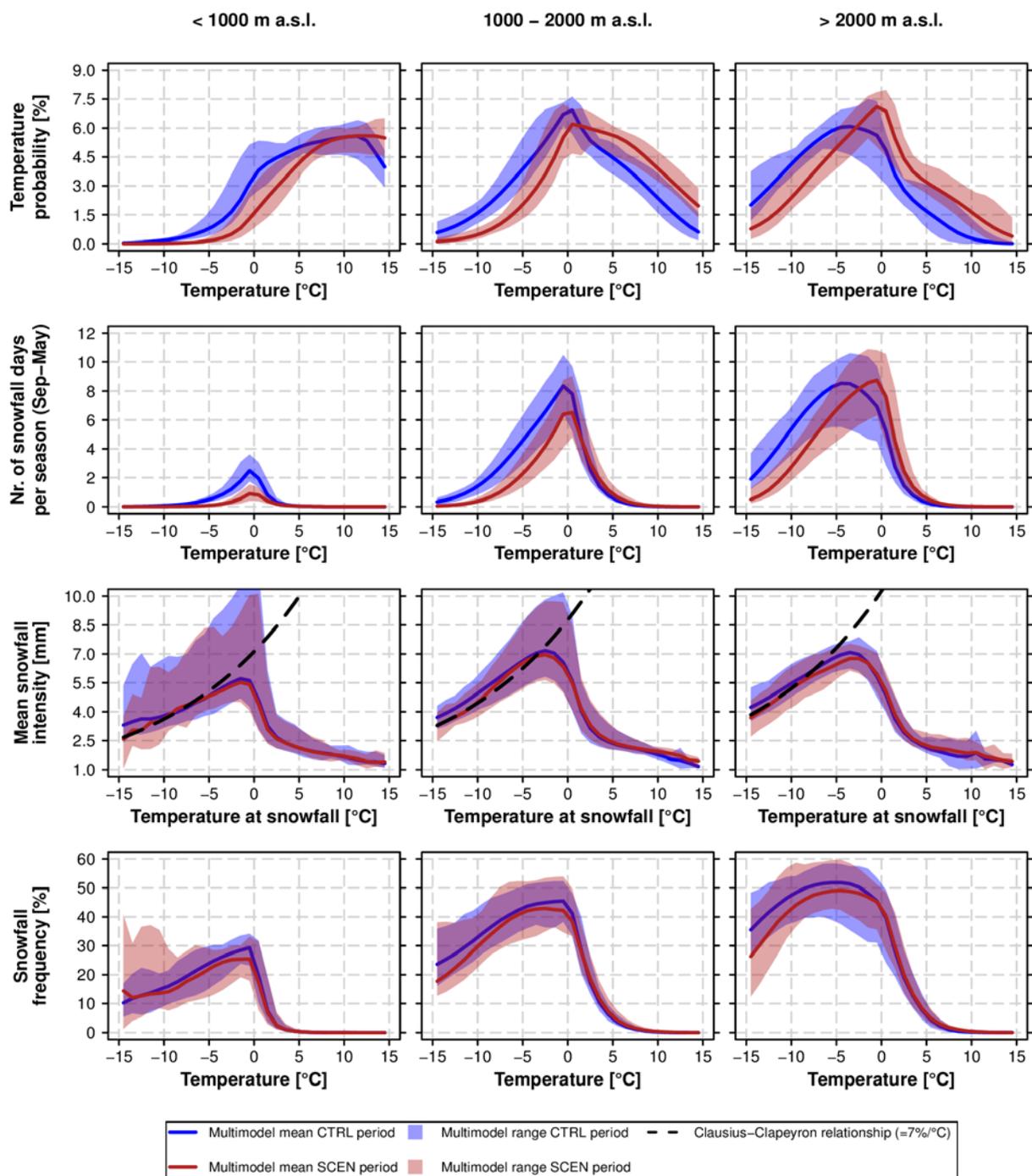
Figure 10 Comparison of temperature probability, snowfall probability and mean snowfall intensity for the CTRL period 1981-2010 and SCEN period 2070-2099 for RCP8.5. The analysis is based on data from the 12 snowfall separated + bias-adjusted RCM simulations (RCM_{sep+ba}) of the reduced model set. The top row depicts the PDF of the daily temperature distribution, while the second row shows the mean number of snowfall days between September and May, i.e., days with S > 1 mm (see Tab. 2), in a particular temperature interval. The third row represents the mean snowfall intensity, S_{int}, for a given snowfall temperature interval. In addition the Clausius-Clapeyron relationship, centred at the -10°C mean S_{int} for SCEN, is displayed by the black dashed line. PDFs and mean S_{int} were calculated by creating daily mean temperature bins of width 1 °C.
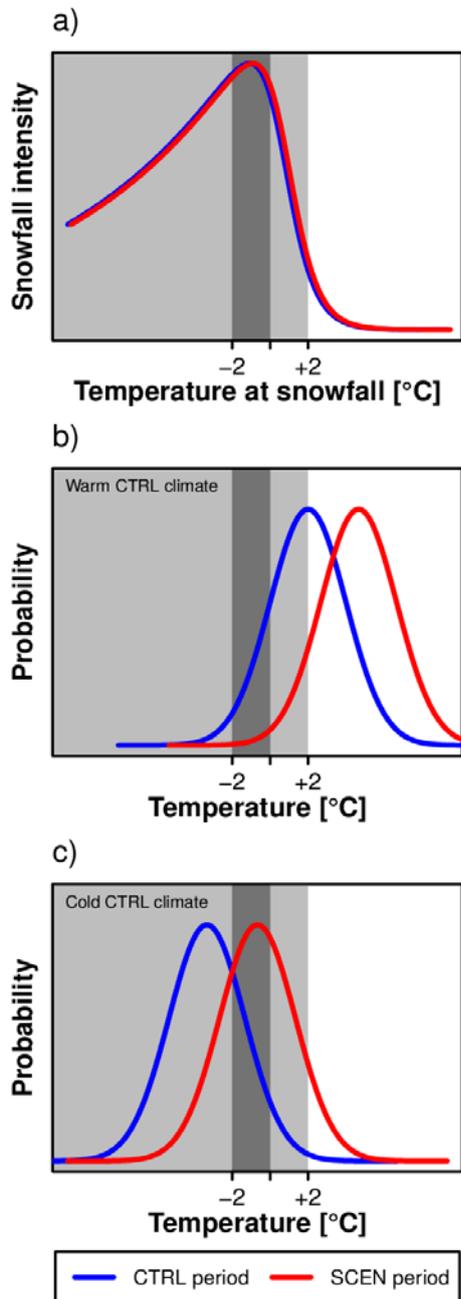
1092

1093

Figure 11 Schematic illustration of the control of changes in snowfall intensity on changes in mean and extreme snowfall. a) Relation between temperature and mean snowfall intensity. b) Daily temperature PDF for a warm control climate (low elevations or transition seasons, i.e., beginning or end of winter). c) Daily temperature PDF for a cold control climate (high elevations or mid-winter). The blue line denotes the historical CTRL period, the red line the future SCEN period. The light grey shaded area represents the overall temperature interval at which snowfall occurs, the dark grey shading shows the preferred temperature interval for heavy snowfall to occur.

1100
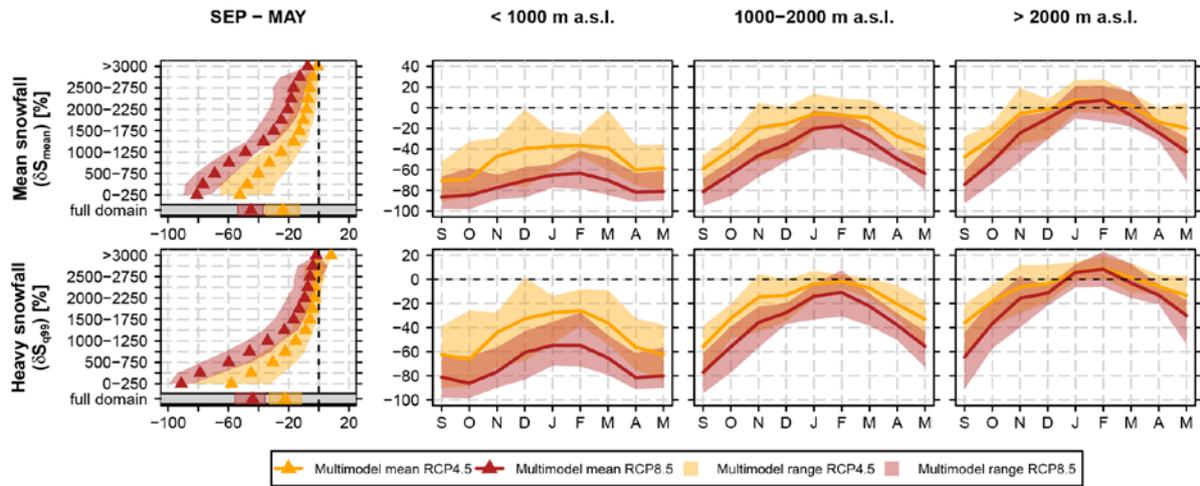
1101

Figure 12 Similar as Figure 8 but showing projected changes of mean snowfall, δS_{mean}, and heavy snowfall, δS_{q99}, for the emission scenarios RCP4.5 and 8.5 and based on the reduced model set. See Fig. S10 for the emission scenario uncertainty of the remaining four snowfall indices. See Fig. S15 for the respective figure based on the full model set.

1106
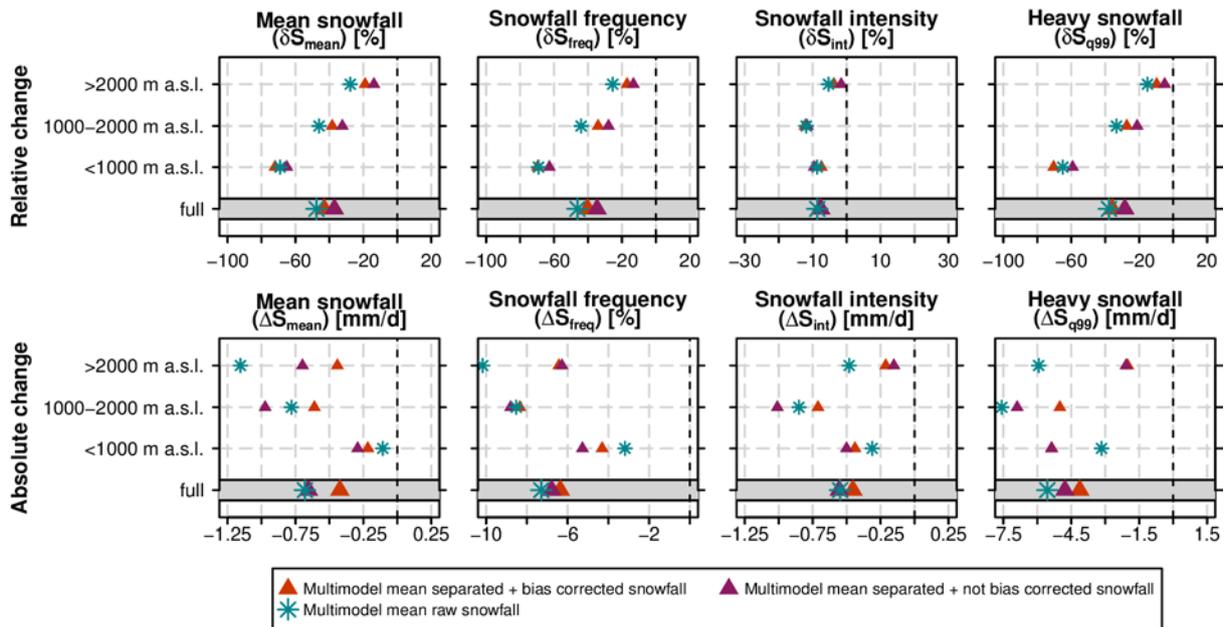
1107
1108

1109   **Figure 13** Relative and absolute changes (SCEN period 2070-2099 with respect to CTRL period 1981-2010) of
1110   mean September-May snowfall indices based on a subset of seven snowfall separated + bias-adjusted
1111   (RCM$_{sep+ba}$), seven snowfall separated + not bias-adjusted (RCM$_{sep+nba}$) and seven raw snowfall RCM simulations
1112   (RCM$_{raw}$) for RCP8.5. Only RCM simulations of the reduced model set providing raw snowfall as output variable
1113   (see Tab. 1) were used in this analysis.

1114

Tables

 Table 1 Overview on the full and the reduced EURO-CORDEX simulations employed in this study. All
 experiments were realized on a grid covering the European domain with a horizontal resolution of approximately
 12 km (EUR-11) and were run for the emission scenarios RCP4.5 and RCP8.5. A subset of nine simulations
 provides raw snowfall, i.e., snowfall flux in kg/m^{2}s, as output variable. The reduced model set excludes
 experiments that are subject to serious shortcomings (see Supplementary Material, Part B). For full institutional
 names the reader is referred to the official EURO-CORDEX website www.euro-cordex.net. Note that the EC-
 EARTH-driven experiments partly employ different realisations of the GCM run, i.e., explicitly sample the
 influence of internal climate variability in addition to model uncertainty.

RCM	GCM	Acronym	Institute ID	Raw snowfall output	Part of reduced model set
ALADIN53	CNRM-CERFACS-CNRM-CM5	CNRM - ALADIN	CNRM	no	X
CCLM4-8-17	CNRM-CERFACS-CNRM-CM5	CNRM - CCLM	CLMcom/BTU	no	X
CCLM4-8-17	ICHEC-EC-EARTH****	EC-EARTH - CCLM	CLMcom/BTU	no	X
CCLM4-8-17	MOHC-HadGEM2-ES	HadGEM2 - CCLM	CLMcom/ETH	no	X
CCLM4-8-17	MPI-M-MPI-ESM-LR	MPI-ESM - CCLM	CLMcom/BTU	no	X
HIRHAM5	ICHEC-EC-EARTH***	EC-EARTH – HIRHAM	DMI	yes	X
RCA4	CNRM-CERFACS-CNRM-CM5	CNRM - RCA	SMHI	yes	X
RCA4	ICHEC-EC-EARTH****	EC-EARTH - RCA	SMHI	yes	X
RCA4	MOHC-HadGEM2-ES	HadGEM2 - RCA	SMHI	yes	X
RCA4	IPSL-IPSL-CM5A-MR	IPSL - RCA	SMHI	yes	X
RCA4	MPI-M-MPI-ESM-LR	MPI-ESM – RCA	SMHI	yes	X
REMO2009	MPI-M-MPI-ESM-LR*	MPI-ESM – REMO	MPI-CSC	yes	X
RACMO22E	ICHEC-EC-EARTH**	EC-EARTH-RACMO	KNMI	yes	-
WRF331F	IPSL-IPSL-CM5A-MR	IPSL - WRF	IPSL-INERIS	yes	-

* r1i1p1 realisation

** r1i1p1 realisation

*** r3i1p1 realisation

**** r12i1p1 realisation

1127 **Table 2** Analysed snowfall indices. The last column indicates the threshold value in the CTRL period for
1128 considering a grid cell in the climate changes analysis (grid cells with smaller values are skipped for the
1129 respective analysis); first number: threshold for monthly analyses, second number: threshold for seasonal
1130 analysis.

Index name	Acronym	Unit	Definition	Threshold for monthly / seasonal analysis
Mean snowfall	S_{mean}	mm	(Spatio-)temporal mean snowfall in mm snow water equivalent (only "mm" thereafter).	1 mm / 10 mm
Heavy snowfall	S_{q99}	mm/d	Grid point-based 99% all day snowfall percentile.	1 mm / 1 mm
Max. 1 day snowfall	S_{1d}	mm/d	Mean of each season's or month's maximum 1 day snowfall.	1 mm / 1 mm
Snowfall frequency	S_{freq}	%	Percentage of days with snowfall S>1mm/d within a specific time period.	1 % / 1 %
Snowfall intensity	S_{int}	mm/d	Mean snowfall intensity at days with snowfall S>1mm/d within a specific time period.	S_{freq} threshold passed
Snowfall fraction	S_{frac}	%	Percentage of total snowfall, S_{tot}, on total precipitation, P_{tot}, within a specific time period.	1 % / 1 %

1131

1132

1133